REPORT ON THE RESULTS
OF ANALYSES PERFORMED ON WELL 8
AT THE SONGS UNITS 2 AND 3
SAN ONOFRE, CALIFORNIA

For

Southern California Edison
P. O. Box 800
Rosemead, California 91770

25 August 1978
40881A

Southern California Edison
P. O. Box 800
Rosemead, California 91770

Attention: Mr. J. Yann

SUBJECT : REPORT ON THE RESULTS OF ANALYSES PERFORMED ON WELL 8 AT THE SONGS UNITS 2 AND 3 SAN ONOFRE, CALIFORNIA

Gentlemen:

In accordance with the technical needs of the project, we have completed our analyses of the potential effects of seismic shaking on the cavity at Well 8, and the resulting potential effects on the adjacent structures. The attached report presents a detailed discussion of the results of the analyses completed.

In brief, the analyses show that the effects of seismic shaking on the cavity will lead to a small, local reduction in stiffness in the soil supporting the adjacent structure during seismic shaking. Further, this reduction in stiffness will be a transient phenomenon lasting, for all practical purposes, for less than one hour after the earthquake. Conservative analyses of the effects of the reduction in soil stiffness on adjacent structures indicate no detrimental effect to the integrity of any adjacent structure or instructure components.

Key personnel involved in the completion of the analyses described in the attached report include Drs. I.M. Idriss, C.Y. Chang, A.G. Masso, and J.N. Mathur of our organization, and Dr. Robert L. McNeill, SCE's project consultant.

We trust that the attached report meets the present needs of the project. Should you have any questions or require clarification of the attached report, please contact the undersigned.

Very truly yours,

John A. Barneich

JAB:ls
Attachments

TABLE OF CONTENTS

FIGURES (Cont'd)

REPORT ON THE RESULTS OF ANALYSES PERFORMED ON WELL 8 AT THE SONGS UNITS 2 AND 3 SAN ONOFRE, CALIFORNIA

1.0 INTRODUCTION

1.1 Purpose and Scope

The purpose of the work described herein is to evaluate the effects of the cavity at dewatering Well 8 on the performance of the adjacent structures in terms of foundation bearing capacity, settlement and response of the structure to seismic loadings at the site of San Onofre Nuclear Generating Station Units 2 and 3, San Onofre, California. The scope of this work includes: (1) evaluation of the effects of seismic loading on the size of the cavity, and (2) evaluation of the effects of the cavity on the stiffness of the soil supporting adjacent structures.

1.2 Approach

There are two basic elements to the approach: (1) the evaluation of the effect of seismic shaking on the size of the cavity in terms of potential physical growth due to a reduction in stiffness of the native soil caused by excess pore pressures transmitted from the liquefied soil fill within the cavity during seismic shaking; and (2) evaluation of the overall reduction in stiffness of the soil supporting the containment structure that could affect the static settlement and bearing capacity of the foundation of the structure before, during and after seismic shaking, and the actual dynamic response of the structure during seismic shaking, based on the initial size of the cavity and its response to seismic shaking as determined from the first element of analysis above.

The first element of the approach was completed by performing a dynamic response and pore-pressure dissipation analysis of the soil-foundation system modeled by finite elements and subjected

to the DBE-level seismic shaking. The second element was accomplished by a simplified analysis of the results of the first analysis described above to determine the reduction in the overall stiffness of the soil supporting the structure. This was based on the relative geometric and stiffness characteristics of the filled cavity and its proximity to the structure and the native soil dominating in the support of the structure.

1.3 Organization of the Report

The summary and conclusions of the work completed are presented in Section 2. The initial conditions at the Well 8 cavity and in the proximity to the Unit 3 containment structure are described in Section 3. Section 4 describes and presents a summary of the results of the dynamic response and pore pressure dissipation analyses. Section 5 describes and presents a summary of the results of the analysis of the effects of the cavity on structures. The supporting data upon which the analyses are based and the details of the analyses are presented in appendices, as follows:

Appendix A - Dynamic Material Properties
Appendix B - Cyclic Strength Characteristics of the San Mateo Sand
Appendix C - Dynamic Response Analyses
Appendix D - Analyses of Excess Pore Water Pressure Generation and Dissipation
Appendix E - Analysis of the Effects on Structures

2.0 SUMMARY AND CONCLUSIONS

As indicated in the sections to follow, the conservative analyses of the maximum effects on the containment structure is a 4 to 5% reduction in overall soil stiffness. Because this is almost an order of magnitude lower than the variation in stiffness accommodated in the design analysis, the cavity will have no effect on the ability of the structure or components to withstand seismic shaking. Similarly, the effects of the cavity on settlement and the bearing capacity of the containment structure were found to be very small and will not affect the integrity of the structure. Further, the tunnel structure was shown by Bechtel Power Corporation to be capable of spanning, without support, the area under the tunnel affected by the cavity. It is therefore concluded that the cavity will have no detrimental effect on the integrity of the tunnel structure. Both the results of the analyses and experience with the San Mateo Sand demonstrate that the effects of softening the San Mateo Sand adjacent to the cavity is a transient phenomenon. The results of the analysis show that, for all practical purposes, the condition in the area of Well 8 and the Unit 3 containment structure have stabilized to the pre-earthquake condition within one hour after the earthquake.

3.0 INITIAL CONDITIONS

The cavity at Well 8 has been thoroughly defined by 192 closely spaced borings in the vicinity of Well 8 and the Unit 3 containment structure as reported in the August 1978 reports documenting the deep drilling and shallow exploration/grouting program for Well 8 (hereinafter referred to as the Well 8 field investigation report). The area explored and discussed in the present report is shown on Figure 1 with respect to adjacent structures. Typical boundaries of the cavity at different elevations are superposed on a plan view drawing of the Unit 3 containment structure in Figure 2a. As noted on Figure 2a, the filled cavity is vertically tabular, and elongates in plan with its long axis oriented roughly 60 degrees west of plant north. This plan geometry or footprint of the filled cavity decreases in size with depth as indicated on Figure 2a. Figure 2b presents the maximum vertical section of the cavity, projected to a plane through the center of the Unit 3 containment structure. The filled cavity does not extend beneath the tendon gallery, as verified by angle borings drilled beneath the structure documented in the Well 8 field investigation report. As indicated in Figures 2a and 2b, the tunnel structure spans the filled cavity.

The soil at the site below the plant grade is a well graded very dense formational sand called the San Mateo Formation Sand, as discussed in Section 2.5.4.2.1.3 of the FSAR. The curves of dynamic shear modulus and damping ratio for this material are given on Figure 3, based on Appendix 2.5D of the FSAR, and as further discussed in Appendix A to this report. As verified in the Well 8 field investigation report, the cavity defined on Figures 2a and 2b is filled with sand and cement grout. The stiffness and damping properties assumed for those materials are presented in Appendix A of this report with those of the sand fill summarized in Figure 4. For purposes of analysis the configuration of the grout and cavity fill sand were simplified

from that defined in the Well 8 field investigation report and as shown on Figure 2b. The cyclic strength characteristics of the San Mateo Sand and the cavity fill sand used in the analyses are described in Appendix B.

4.0 DYNAMIC RESPONSE AND PORE PRESSURE DISSIPATION ANALYSES

4.1 Approach

One of the approaches used to evaluate the potential effect of the soil filled cavity during seismic shaking on the adjacent structures is to assess the nature of generation and dissipation of excess pore water pressures in the soil foundation. Time histories of excess pore water pressures can then be used to evaluate changes of static and dynamic stiffnesses of the foundation soil. The basic approach used in analysis of generation and dissipation of excess pore water pressure during and after seismic shaking involves the following two main steps:

1. Dynamic Response Analyses - Dynamic response analyses of a representative soil-structure system due to the postulated DBE were conducted to obtain time histories of induced shear stress in every element of the soil-foundation system.

2. Analyses of Generation and Dissipation of Excess Pore Water Pressure During and After Seismic Shaking - Using the time histories of induced shear stress computed in Step 1 and cyclic strength, pore water pressure generation and permeability characteristics of the foundation soil, generation and dissipation of excess pore water pressure in the soil-foundation system during and after seismic shaking were computed using the finite-element procedure.

Analysis procedures and results are described in detail in Appendices C and D. A brief summary of these analyses is presented in subsequent sections.

4.2 Dynamic Response Analyses

The basic soil-structure interaction study can be made using the finite element method (Idriss et al, 1973; Lysmer et al, 1976) in which soil and structures are modeled in a combined system. For this study, the dynamic response of the soil-structure system was

evaluated using the computer program FLUSH. The FLUSH program (Lysmer et al, 1976) uses the method of complex moduli (Lysmer et al, 1974). The strain-dependent nature of the shear modulus and damping of the soils shown in Figures 3 and 4 are accounted for by the use of equivalent linear soil properties (Idriss et al, 1969) using an interative procedure to obtain values of modulus and damping that are compatible with the effective strains in each soil element. The main features of the FLUSH program include the following:

1. A three-dimensional approximation of soil-structure interaction effects. This is accomplished by using energy-absorbing viscous dashpots to provide radiation damping in the third direction, i.e., these dashpots remove energy radiating in the third direction.

2. Use of transmitting boundaries which greatly reduce the number of elements required to minimize boundary effects, thus allowing for the use of a finer element mesh in the area of interest (in this case the area of the cavity at Well 8 and the Unit 3 containment structure) while still remaining within the core capacity of the computer.

4.2.1 Finite Element Model

The finite element soil-structure model used in the FLUSH analysis is shown in Figure 5. This model corresponds to the maximum vertical section of the filled cavity projected to a plane through Well 8 and the center of the Unit 3 containment structure. The model incorporates the Unit 3 containment structure, the tunnel structure, the grout and the soil filled cavity.

The containment structure was idealized by a stick model located at the center of the structure. The model parameters are described in Appendix A.

The model conservatively assumed the axis of the containment structure to be the axis of symmetry; thus, assuming cavities on both sides of the containment structure. A transmitting boundary is provided at the left side of the model. Viscous dashpots are provided for the foundation mat to absorb energy radiating in the third direction. The width of the model is conservatively assumed to be 25 feet corresponding to the maximum width of the cavity (see Figure 2a).

4.2.2 Input Motion

The artificial time history of acceleration representing the postulated DBE previously developed for the San Onofre Nuclear Generating Station was used as the control motion for the response computations. The control motion is specified at the finished grade of the plant site. The accelerogram has a peak aceleration of 2/3g and a total duration of approximately 80 seconds.

4.2.3 Analyses Results

Results of dynamic analyses include time histories of acceleration and stress at selected locations in the soil-structure system. The analysis results are presented in Appendix C. The time histories of induced shear stress were converted to equivalent uniform stresses for each element and used to define excess pore water pressure generation characteristics during seismic shaking described in the following section.

4.3 Analyses of Generation and Dissipation of Excess Pore Water Pressure

During the last decade, analysis of the liquefaction and excessive cyclic straining potential has been based on undrained conditions in which the effects of the redistribution and dissipation of pore pressures on the liquefaction potential of the soil mass are assumed to be insignificant. Recent advance in

analysis techniques (Seed et al, 1975; Rahman et al, 1976; and Booker et al, 1976) enables analyses to couple both generation and dissipation of pore water pressures in the evaluation of the liquefaction potential of the soil mass during and after seismic shaking. Details of analysis procedures are described in Appendix D.

For this study, the analysis of pore water pressure generation and dissipation in the foundation soil was conducted using the computer program GADFLEA (Booker, Rahman and Seed, 1976). The GADFLEA program was developed based on the finite element method for plane strain or axisymmetric problems.

In this study, both axisymmetric and plane strain analyses were conducted. Detailed discussions of the analysis models are presented in Appendix D. The basic analysis was made for the axisymmetric case to define pore water pressure redistribution beneath the Unit 3 containment structure. The plane strain solution was used as a basis to estimate pore water pressure redistribution in the direction away from the containment structure. Based on the results of the axisymmetric and plane strain solutions, pore water pressure dissipations in directions other than the analysis section were conservatively estimated. The estimates were based on comparisons of lengths of drainage path and filled cavity size.

Several conservative assumptions were made in the analyses conducted. These assumptions include: (1) the geometry of the cavity was assumed to be two-dimensional (plane strain or axisymmetric case); and (2) the shortest drainage path beneath the containment structure in the analysis section was assumed to be along the basemat of the containment structure, i.e., a drainage path equal to the diameter of the basemat. The first assumption implies that the volume of the pore pressure generating source is much greater than the actual size of the

cavity (the plane strain case assumed that the length of the cavity is infinite in the third direction perpendicular to the analysis section; the axisymmetric case assumed that the cavity is a cone with the axis of Well 8 as the axis of revolution and a cross-section equal to the maximum section of the cavity). The conservativeness of this assumption has been quantified in Appendix D. The second assumption increases time required for dissipation of excess pore pressures and overestimates pore pressure at any given time during periods of dissipation as compared to the actual field condition. Figure 1 indicates that the bases of foundation mats for structures adjacent to Well 8 except the Unit 3 containment structure will be situated above the ground water table. Thus, any potential excess pore water pressures generated within the cavity should dissipate radially and quickly in the immediate vicinity of the well.

Detailed results of the analyses are presented in Appendix D. A brief summary of these results in terms of pore water pressure ratio (ratio of excess pore water pressure to effective vertical stress) is presented in Figures 6 through 14. Figure 6 shows the distribution of pore water pressure ratio at t = 12 seconds after the beginning of seismic shaking on a vertical cross-section through the axis of Well 8 and the center of the Unit 3 containment structure. Figure 7 shows the distribution of pore water pressure ratio on a horizontal section through the base of the tendon gallery of the containment structure (elevation -10 feet) at t = 12 seconds. Figures 6 and 7 indicate that at t = 12 seconds the native San Mateo Sand surrounding the cavity and with a maximum thickness of approximately 6 feet reaches a condition of initial liquefaction (pore pressure ratio = 1.0). The zone of initial liquefaction does not increase during and after subsequent seismic shaking.

Figures 8 through 11 summarize the distributions of pore water pressure ratio toward the end of seismic shaking (t = 80 seconds)

i.e., the end of the pore water pressure generation period. The zone of the maximum pore water pressure (ratio = 1.0) should gradually reduce during subsequent dissipation and redistribution. Figure 8 shows the distribution on the vertical cross-section through the containment structure. Figures 9, 10 and 11 show the distributions on the horizontal sections through the base of the tendon gallery (elevation -10), elevations -60 feet and -100 feet, respectively.

Figures 12 and 13 show the pore pressure distributions at t = 3 minutes for the vertical cross-section and the horizontal section through the base of the tendon gallery, respectively. The distributions at t = 3 minutes indicate approximately the maximum pore pressure dissipated into the native San Mateo Sand formation. It is noted that at t = 3 minutes the zone of pore pressure ratio equal to one is reduced significantly in size so that the area of initial liquefaction in the native soil no longer exists and that much of the cavity fill soil has stabilized from a condition of liquefaction.

Figure 14 shows the distribution of pore pressure ratio at t = 60 minutes when the excess pore pressures in both the soil fill within the cavity and the native sand are practically dissipated.

The results of the generation and dissipation analyses are used to assess the effects on structures described in Section 5. The results of these analyses as summarized in Figures 6 through 14 show that liquefaction of the cavity fill sand and the reduction in confining pressure on the adjacent native soils due to pore pressure dissipation represent a transient condition. As indicated in Figure 14, for all practical purposes, the condition in the area of Well 8 and the Unit 3 containment structure have stabilized to the pre-earthquake condition within one hour after the earthquake. This result is consistent with the geometry and

characteristics of the filled cavity and experience with the San Mateo Sand over the past few years, in both laboratory and field situations. This experience leads to the conclusion that the sand would fail under such conditions by particulating grain-by-grain. Experience and field and laboratory data further show that, in going from its natural state to its particulate state, the San Mateo Sand bulks (increases in volume) by about 20%. Thus the tendency for the natural material to particulate would be accompanied by a tendency to bulk which, in turn, would be resisted by the sand and grout already filling the cavity.

5.0 POTENTIAL EFFECTS ON STRUCTURES

The details of the analyses completed to evaluate the effects of the cavity at Well 8 on the adjacent Unit 3 containment structure are described in Appendix E. Basically, the analyses described consist of comparing the loss of stiffness of the San Mateo Sand due to the cavity to the stiffness of the native San Mateo Sand that dominates in the static and seismic response of the structure. This comparison was quantified by a ratio of various properties of the cavity to those of the dominant supporting soil as defined in Appendix E. These properties include relative areas at the base of the structure and relative weighted volumes to model the translation response (static settlement and dynamic horizontal and vertical translation response) of the structures as related to the relative compression and inertia of the cavity and supporting soil, respectively. For the rotational responses, (differential settlement and dynamic rocking response) the properties include the relative area-moments of inertia of slices (weighted with depth), and the relative weighted mass moments of inertia. These related to the relative overturning (rotational compression) and rotational inertia of the cavity and supporting soil, respectively.

The property ratios, as a percent reduction in overall stiffness of the soil mass supporting the structure, were calculated using the results of the pore pressure dissipation analyses, conservatively assuming zero stiffness for soil within the contour of excess pore pressure equal to 1 and reduced stiffness for all soil exhibiting excess pore pressure as described in Appendix E. These calculations yield results as summarized in Table 1. These results indicate a maximum effect of between 4 and 5% reduction in stiffness.

The dynamic response analysis completed for the design of Unit 3 containment was made assuming a $\pm$30% variation in stiffness parameters. The maximum 4 to 5% reduction in stiffness as

calculated by the analyses is substantially below that variation, and is therefore well within the margin of safety for the design. The static settlement of the Unit 3 containment structure was estimated to be less than 1/2 inch. Assuming this settlement to increase in proportion to the changes indicated on Table 1, the maximum 5 to 6% change in settlement calculated by the analyses yields a very small theoretical increase in settlement (less than 1/10 inch).

A second analysis of the effect of the cavity on the settlement of the structure was made by calculating the potential change in volume of the soil beneath the containment structure due to the drainage of excess pore pressures. Specifically, this volume was calculated by multiplying volumetric strains reported by Lee and Albaisa (1974) to the volumes of soil enclosed by contours of constant pore pressure within the soil dominating the support of the structure as defined in Appendix E. The maximum potential settlement of the structure due to this phenomenon was then calculated by assuming the structure to tilt to accommodate this change in volume with no settlement on the side of the containment away from the cavity, and maximum settlement on the side of the containment near the cavity. This settlement was also calculated to be less than 1/10 inch. The factor of safety against bearing failure for the containment is in excess of 100 (Section 2.5.4.10.3 of the FSAR). A maximum 5 to 6% reduction in this factor would still yield a factor of safety of greater than 100.

The effect of the cavity on the tunnel structure was based on the results of the pore-pressure dissipation analyses presented above. This was done by conservatively assuming that the tunnel would be unsupported in the area of the cavity within the maximum extent of the 0.5 pore-pressure-ratio contour at any point below the tunnel, as indicated on Figure 15 by the cross-hatched area. The tunnel was then checked for its spanning capabilities by

Bechtel Power Corporation. These calculations confirmed that the tunnel can span, unsupported, the cross-hatched area on Figure 15.

REFERENCES

Booker, J. R., Rahman, M. S., and Seed, H. B. (1976) "GADFLEA - A Computer Program for the Analysis of Pore pressure Generation and Dissipation During Cyclic or Earthquake Loading", Report No. EERC 76-24, Earthquake Engineering Research Center, University of California, Berkeley, October.

Casagrande, A. (1976) "Liquefaction and Cyclic Deformation of Sands - A Critical Review", Harvard Soil Mechanics Series No. 88, Harvard University, Cambridge, Mass.

DeAlba, P., Chan, C. K., and Seed, H. B. (1975) "Determination of Soil Liquefaction Characteristics by Large-Scale Laboratory Tests", Report No. EERC 75-14, Earthquake Engineering Research Center, University of California, Berkeley, May.

Idriss, I. M., Dezfulian, H. and Seed, H. B. (1969) "Computer Programs for Evaluating the Seismic Response of Soil Deposits with Nonlinear Characteristics Using Equivalent Linear Procedures", Research Report, Geotechnical Engineering, University of California, Berkeley, April.

Idriss, I. M., Lysmer, J., Hwang, R., and Seed, H. B. (1973) "QUAD-4 A Computer Program for Evaluating the Seismic Response of Soil Structures by Variable Damping Finite Element Procedures", Report No. EERC 73-16, Earthquake Engineering Research Center, University of California, Berkeley.

Lee, K. L., and Albaisa, A. (1974) "Earthquake Induced Settlements in Saturated Sands", Journal of the Geotechnical Engineering Division, ASCE, Vol. 100, No. GT4, April.

Lysmer, J., Udaka, T., Tsai, C.-F., and Seed, H. B. (1975) "FLUSH - A Computer Program for Approximate 3-D Analysis of Soil-Structure Interaction Problems", Report No. EERC 75-30, Earthquake Engineering Research Center, University of California, Berkeley.

Rahman, M. S., Seed, H. B., and Booker, J. R. (1976) "Liquefaction Analysis for Offshore Oil Tanks", Geotechnical Engineering Report, University of California, Berkeley, September.

Schnabel, P. B., Lysmer, J., and Seed, H. B. (1972) "SHAKE: A Computer Program for Earthquake Response Analysis of

Horizontally Layered Sites", Report No. EERC 72-12, Earthquake Engineering Research Center, University of California, Berkeley, December.

Seed, H. B. (1976) "Evaluation of Soil Liquefaction Effects on Level Ground During Earthquakes", State-of-the-Art Paper prepared for Symposium on Soil Liquefaction, ASCE National Convention, Philadelphia, Pennsylvania, October.

Seed, H. B., and Booker, J. R. (1976) "Stabilization of Potentially Liquefiable Sand Deposits Using Gravel Drain Systems", Report No. EERC 76-10, Earthquake Research Center, University of California, Berkeley, April.

Seed, H. B., and Idriss, I. M. (1970) "Soil Moduli and Damping Factors for Dynamic Response Analysis", Report No. EERC 70-0, Earthquake Engineering Research Center, University of California, Berkeley.

Seed, H. B., Idriss, I. M., Makdisi, F., and Banerjee, N. (1975) "Representation of Irregular Stress Time Histories by Equivalent Uniform Stress Series in Liquefaction Analyses", Report No. EERC 75-29, Earthquake Engineering Research Center, University of California, Berkeley, October.

Seed, H. B., Martin, P. P., and Lysmer, J. (1975) "The Generation and Dissipation of Pore Water Pressures During Soil Liquefaction", Report No. EERC 75-26, Earthquake Engineering Research Center, University of California, Berkeley, August.

TABLE 1

SUMMARY OF THE MAXIMUM EFFECT OF THE WELL 8 CAVITY ON THE UNIT 3 CONTAINMENT STRUCTURE

Response Element	Condition		
	Normal Operation (initial Condition)	During DBE	Within 60 mins. After DBE
Maximum Change in Structure Settlement			
Total (vertical translation)	<1%	4%	5%
Differential (rotation)	<1%	5%	6%
Maximum Change in Dynamic Stiffness of the Foundation Soil Affecting Dynamic Response of the Structure			
Vertical and Horizontal Translation		4%	
Rocking		5%	

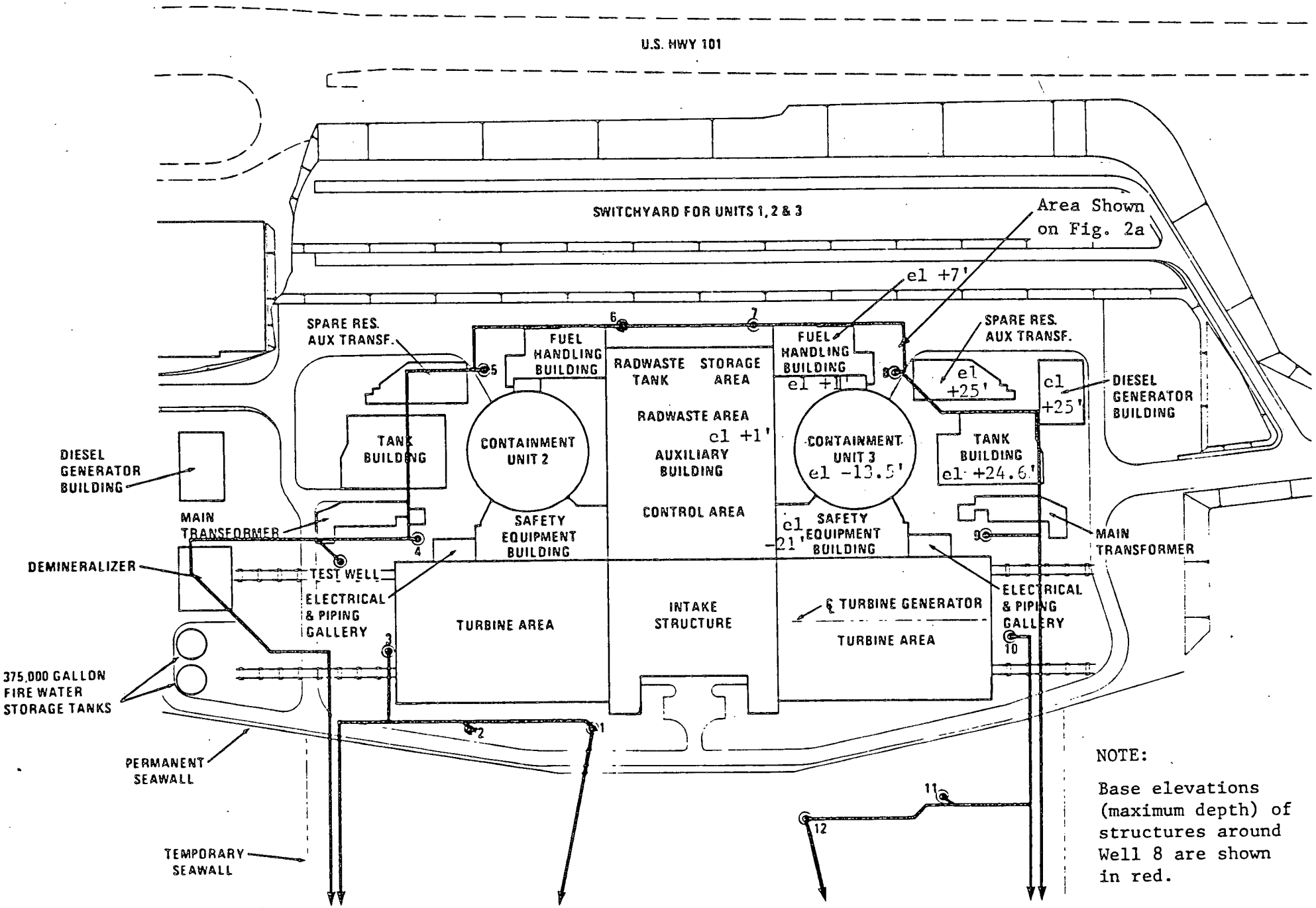

NOTE:

Base elevations (maximum depth) of structures around Well 8 are shown in red.

Fig. 1 PLOT PLAN

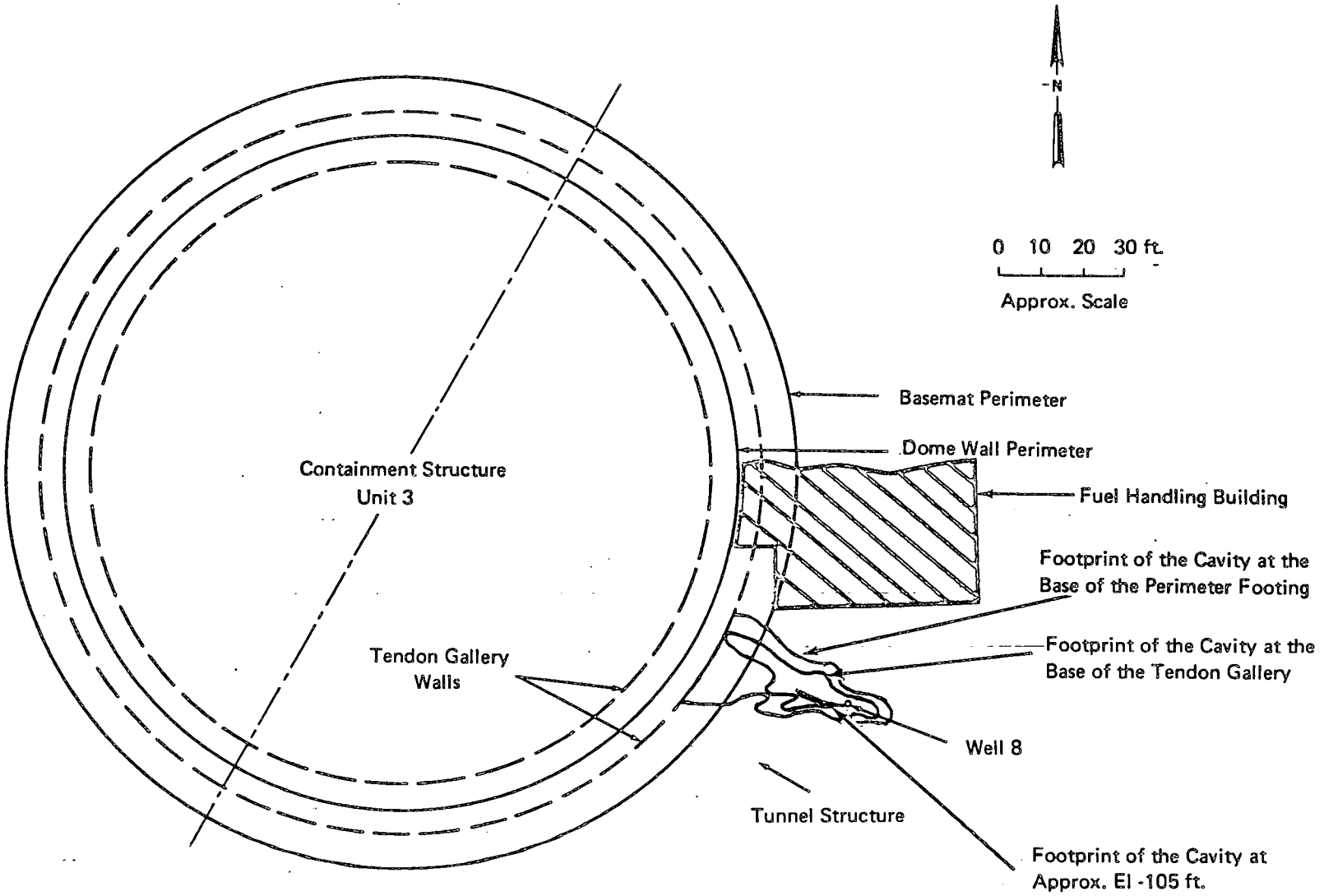

Fig. 2a INTERPRETED PLAN SECTIONS OF THE CAVITY AND THE CONTAINMENT STRUCTURE UNIT 3

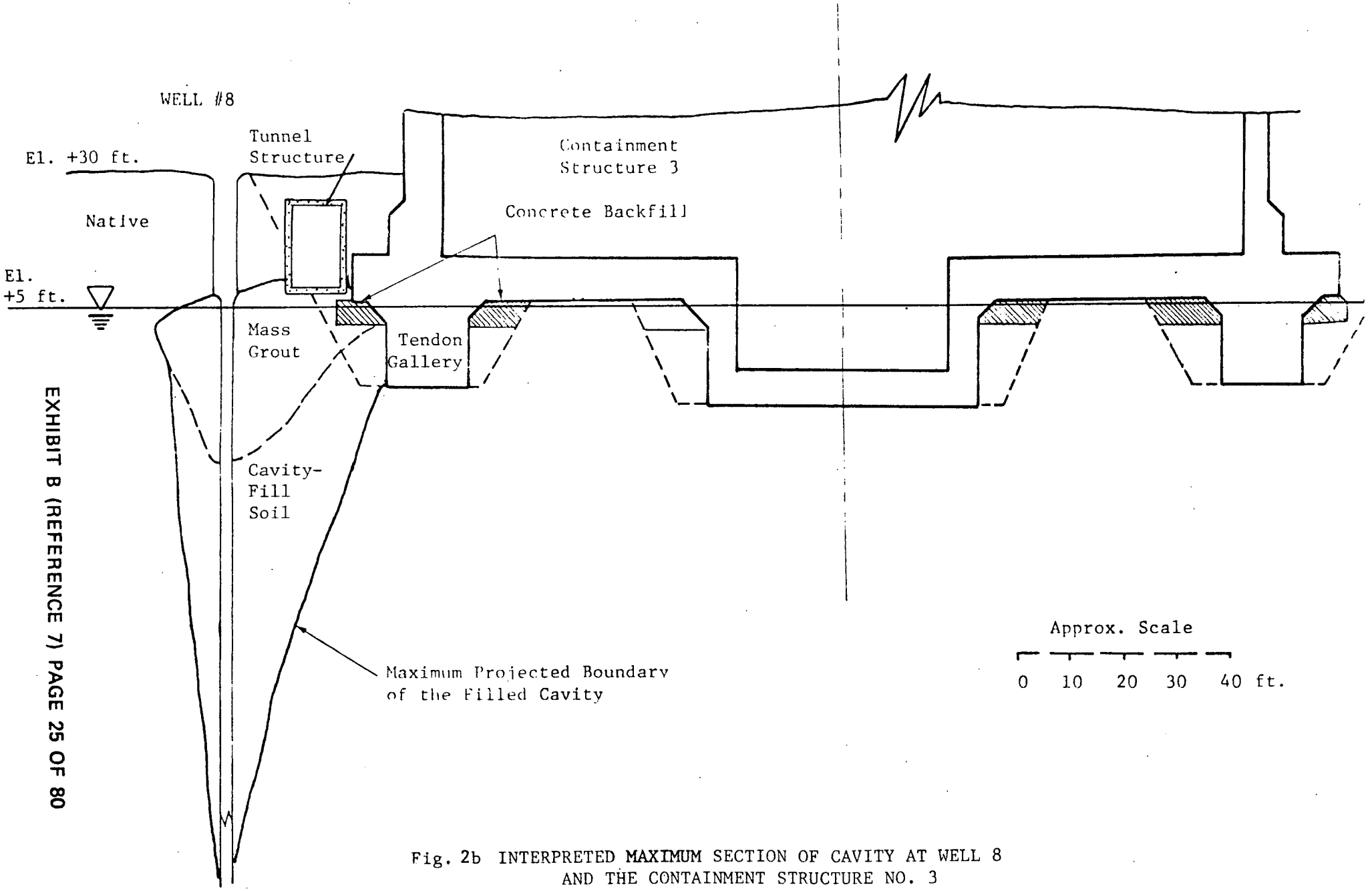

Fig. 2b INTERPRETED MAXIMUM SECTION OF CAVITY AT WELL 8 AND THE CONTAINMENT STRUCTURE NO. 3

EXHIBIT B (REFERENCE 7) PAGE 25 OF 80

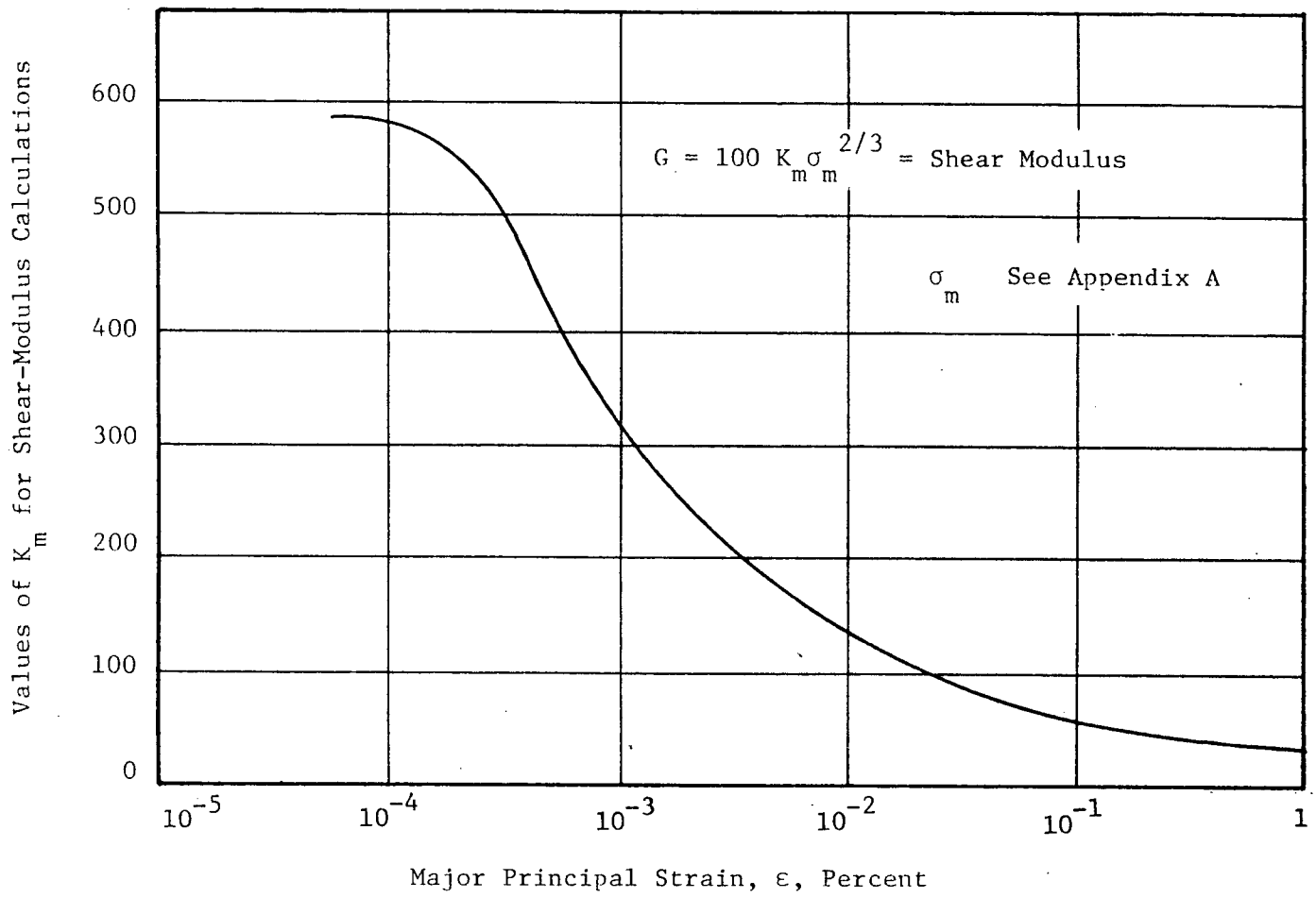

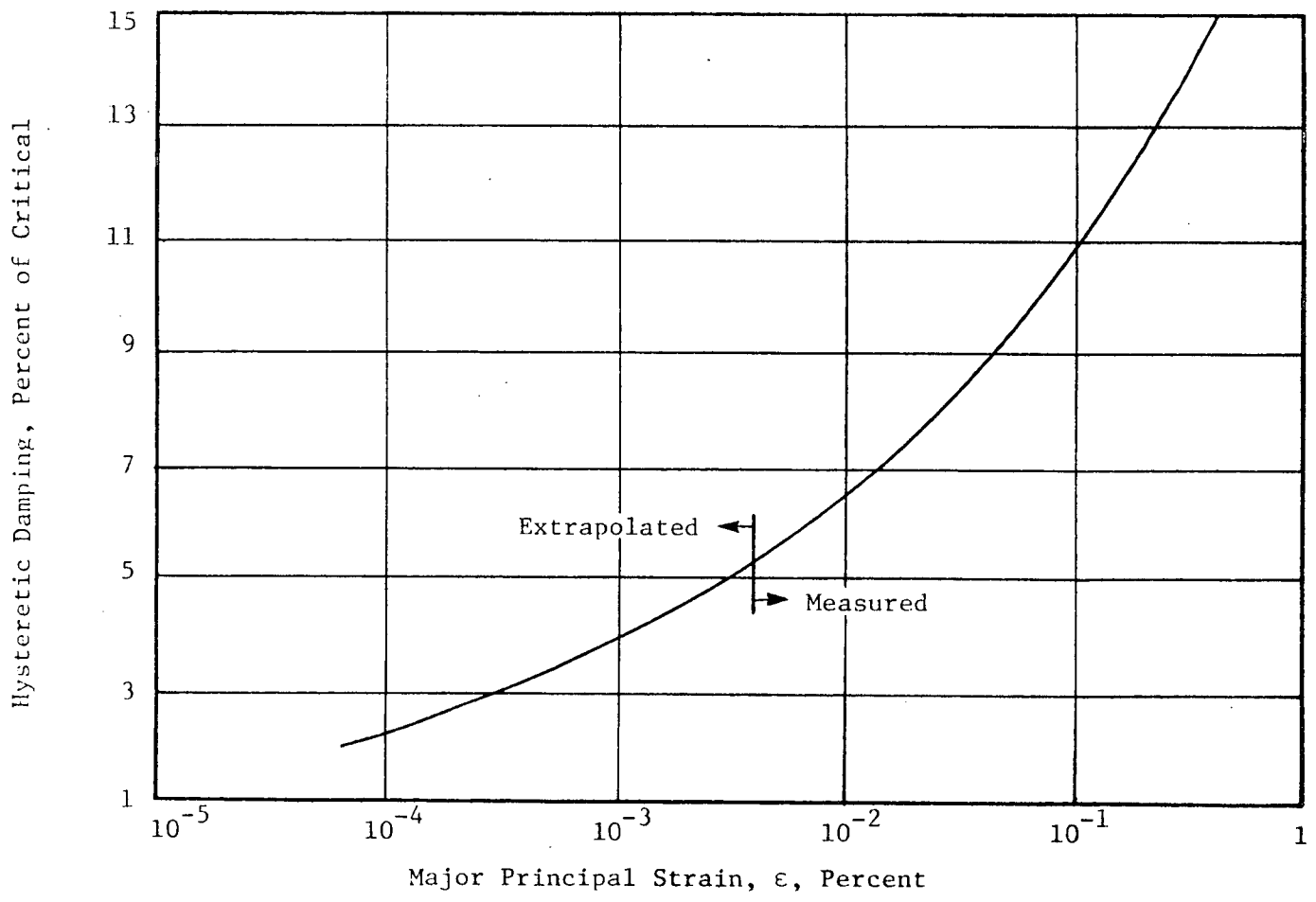

EXHIBIT B (REFERENCE 7) PAGE 26 OF 80

Fig. 3 STIFFNESS AND DAMPING PARAMETERS FOR THE NATIVE SAN MATEO SAND

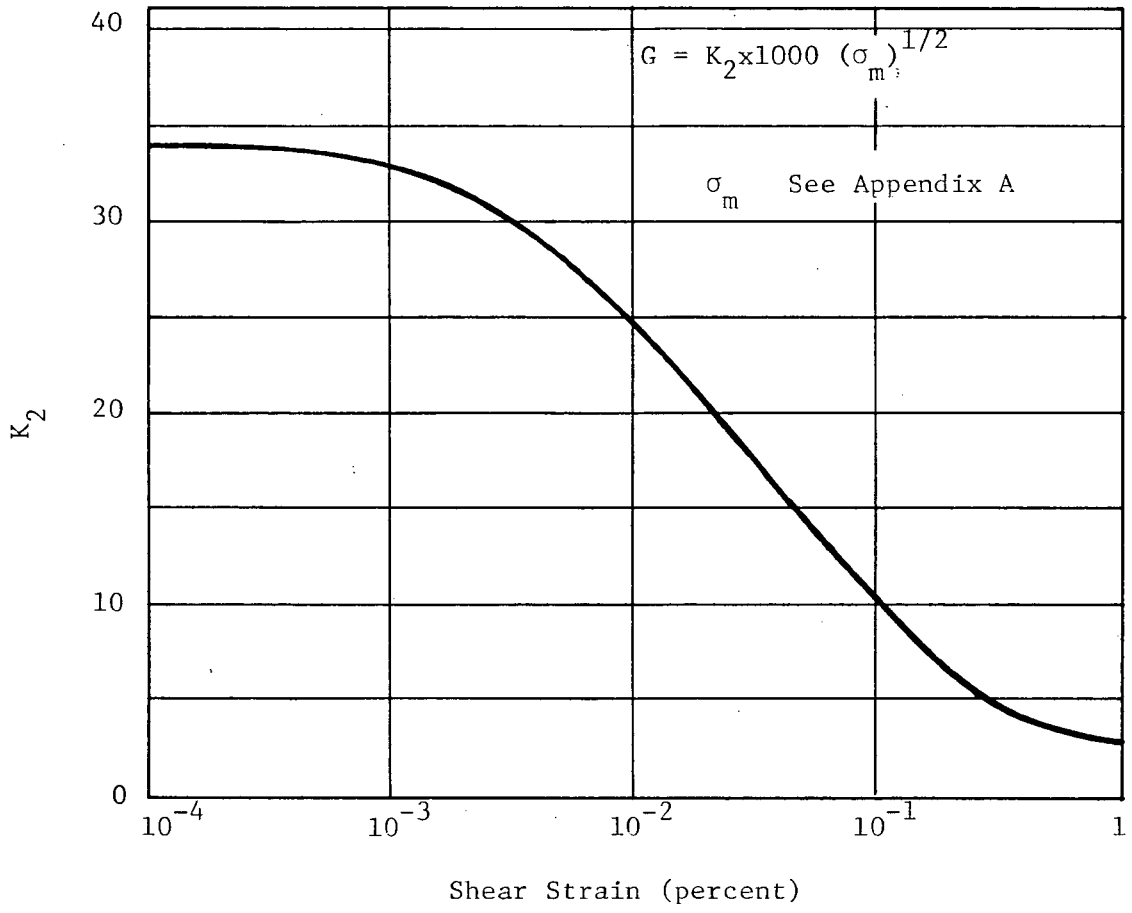

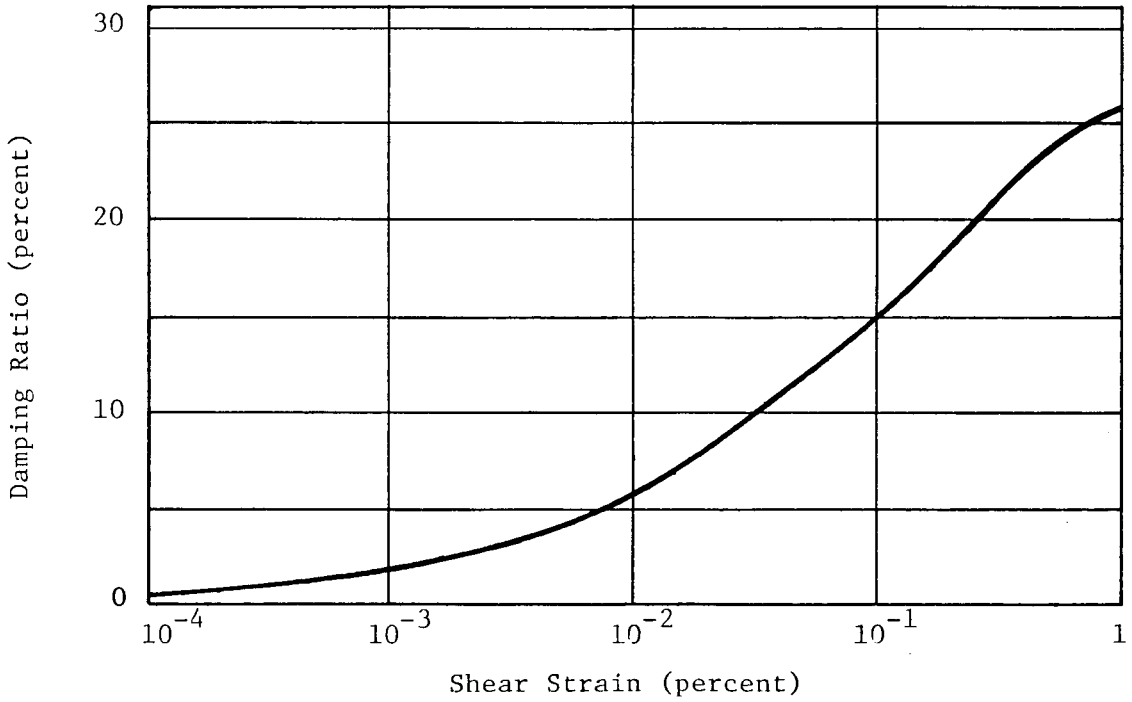

Fig. 4 SHEAR MODULUS AND DAMPING VALUES FOR CAVITY-FILL SAND

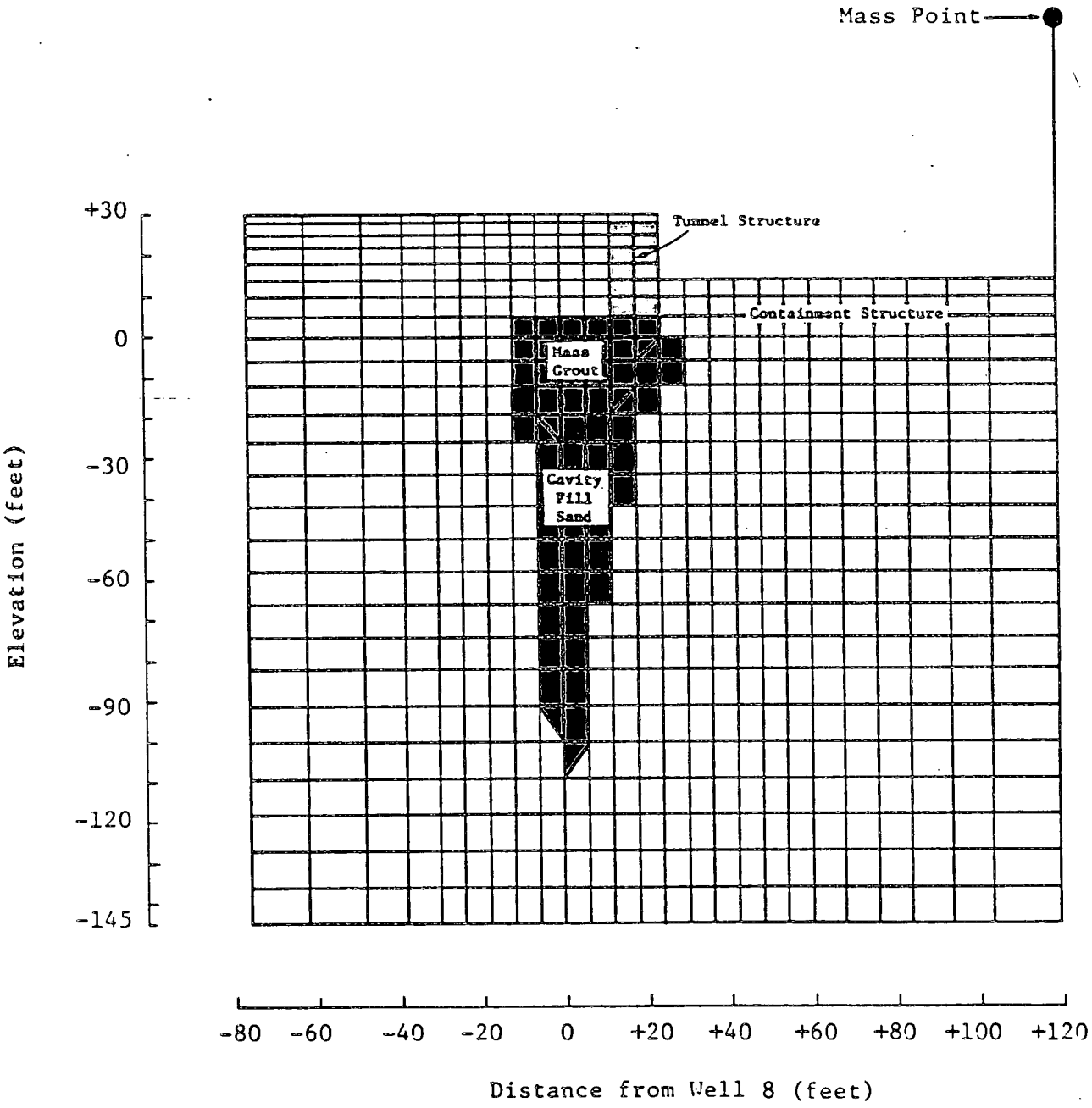

Fig. 5 FINITE ELEMENT MESH USED IN ANALYSIS

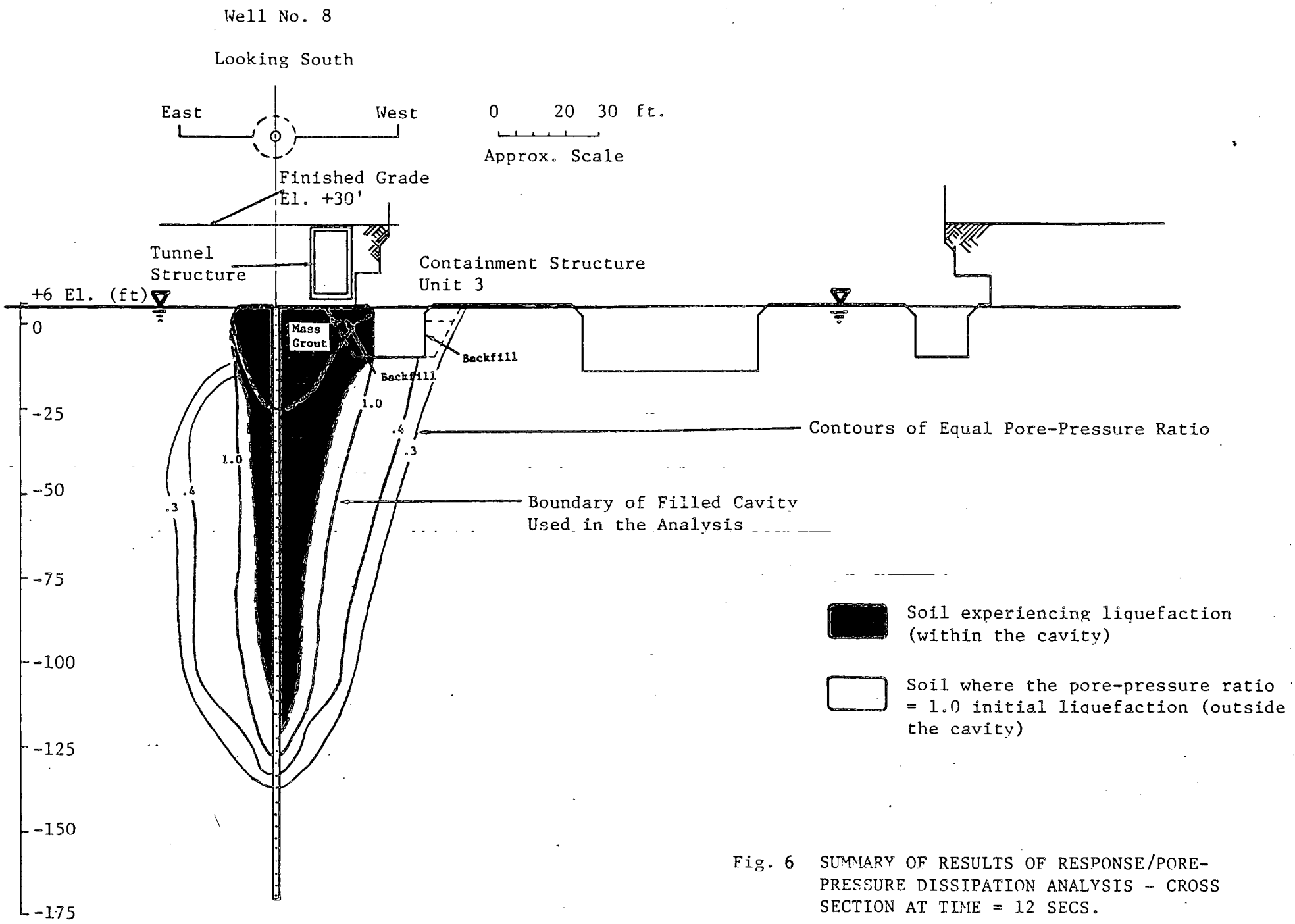

Fig. 6 SUMMARY OF RESULTS OF RESPONSE/PORE-PRESSURE DISSIPATION ANALYSIS - CROSS SECTION AT TIME = 12 SECS.

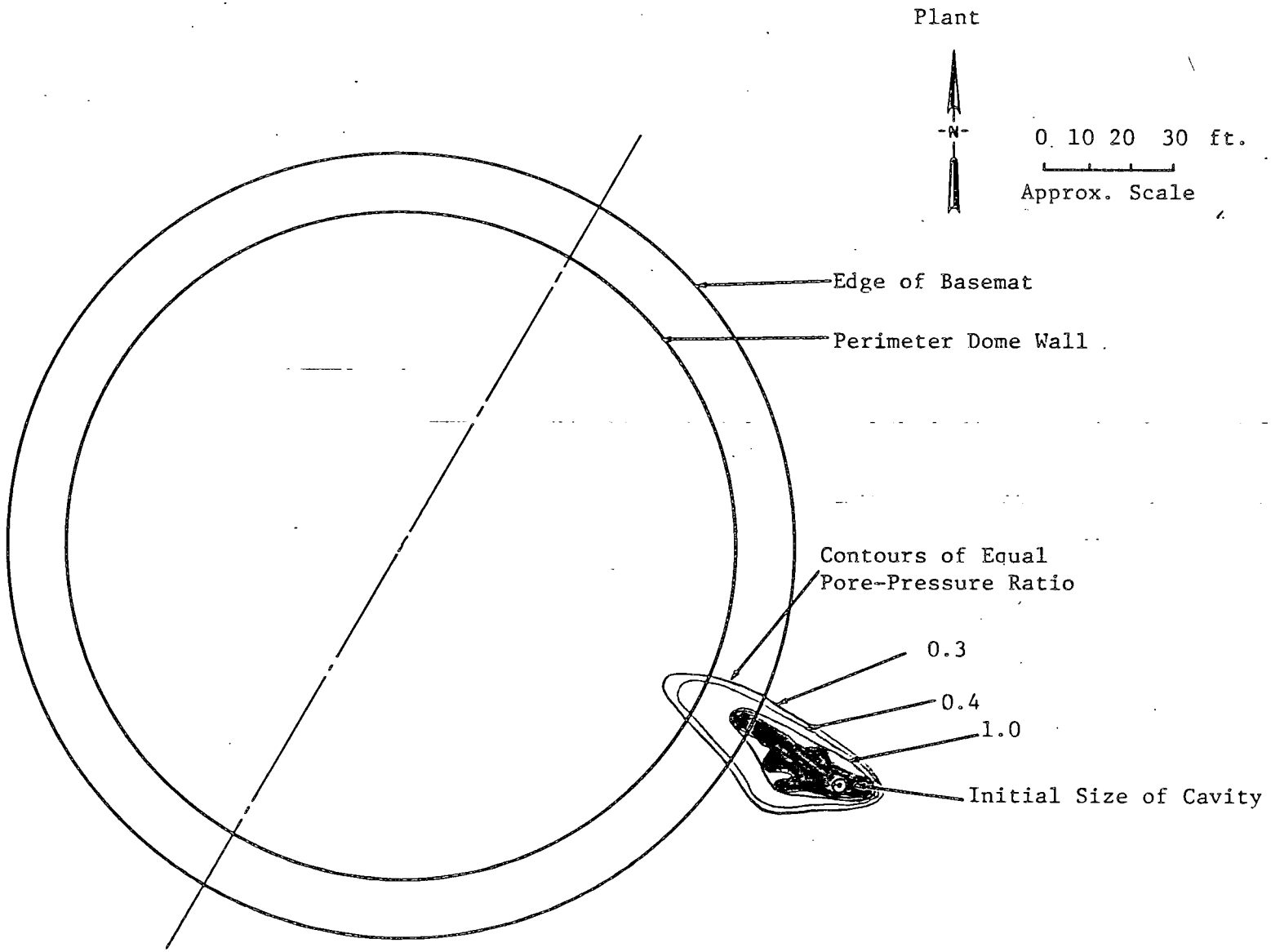

Fig. 7 SUMMARY OF RESULTS OF THE RESPONSE/PORE-PRESSURE DISSIPATION ANALYSIS - PLAN SECTION AT THE BASE OF THE TENDON GALLERY AND TIME = 12 SECS.

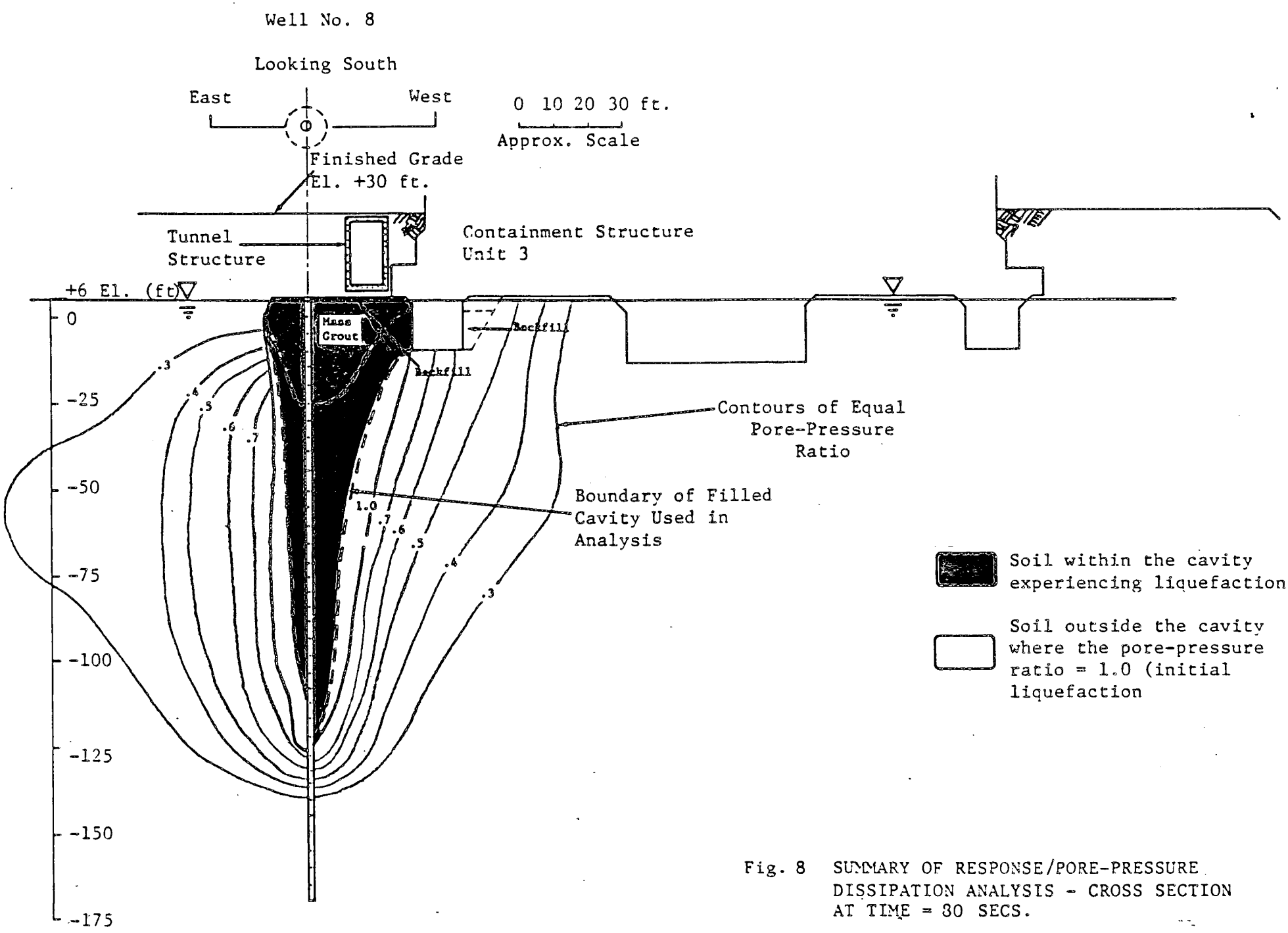

Fig. 8 SUMMARY OF RESPONSE/PORE-PRESSURE DISSIPATION ANALYSIS - CROSS SECTION AT TIME = 30 SECS.

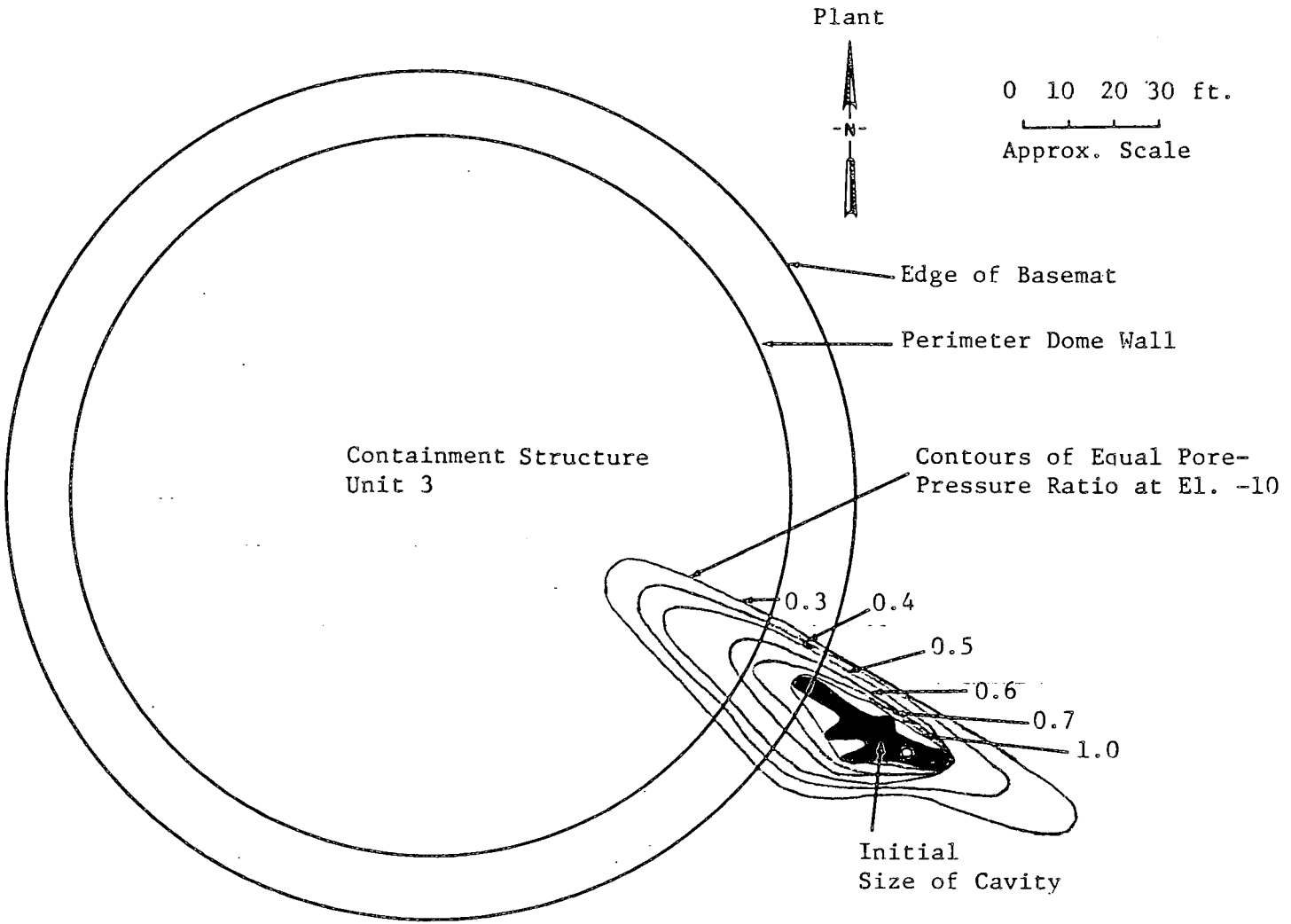

Fig. 9 SUMMARY OF THE RESULTS OF THE RESPONSE/PORE-PRESSURE DISSIPATION ANALYSIS - FOR THE BASE OF THE TENDON GALLERY AND TIME = 80 SECS.

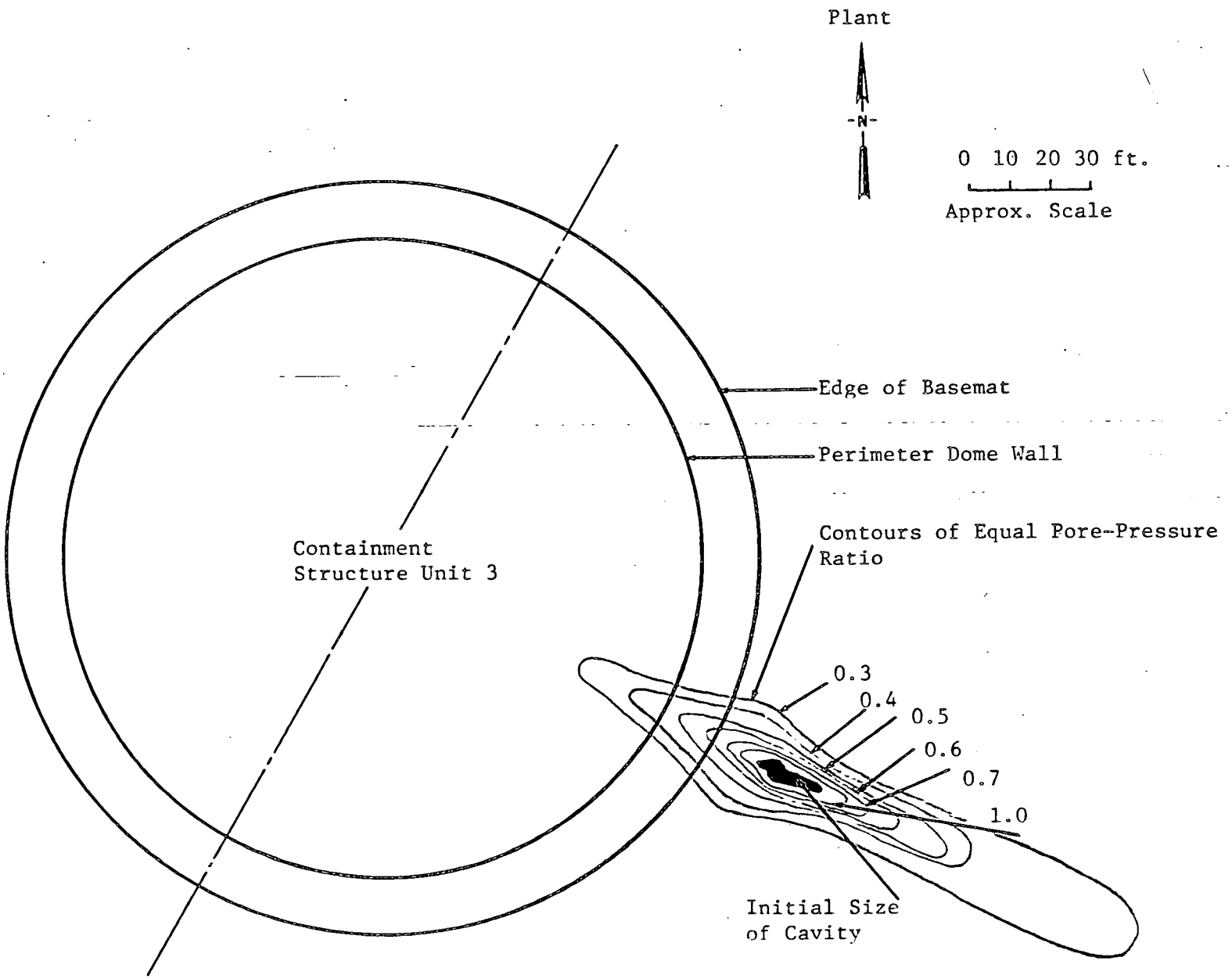

Fig. 10 SUMMARY OF RESULTS OF THE RESPONSE/PORE-PRESSURE DISSIPATION ANALYSIS - FOR EL. -60 AND TIME = 80 SECS.

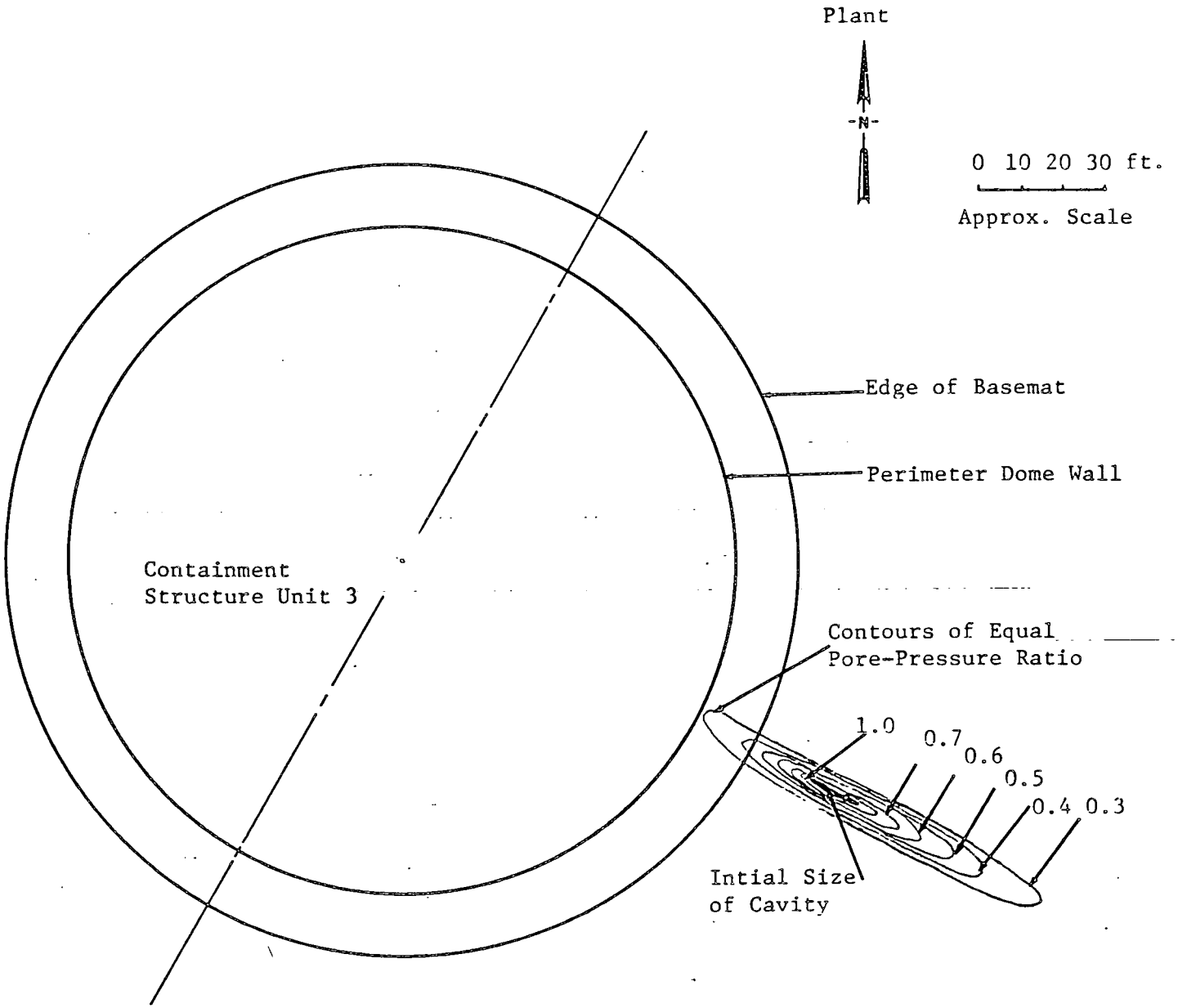

Fig. 11 SUMMARY OF RESULTS OF THE RESPONSE/PORE-PRESSURE DISSIPATION ANALYSIS - FOR EL. -100 AND TIME = 80 SECS.

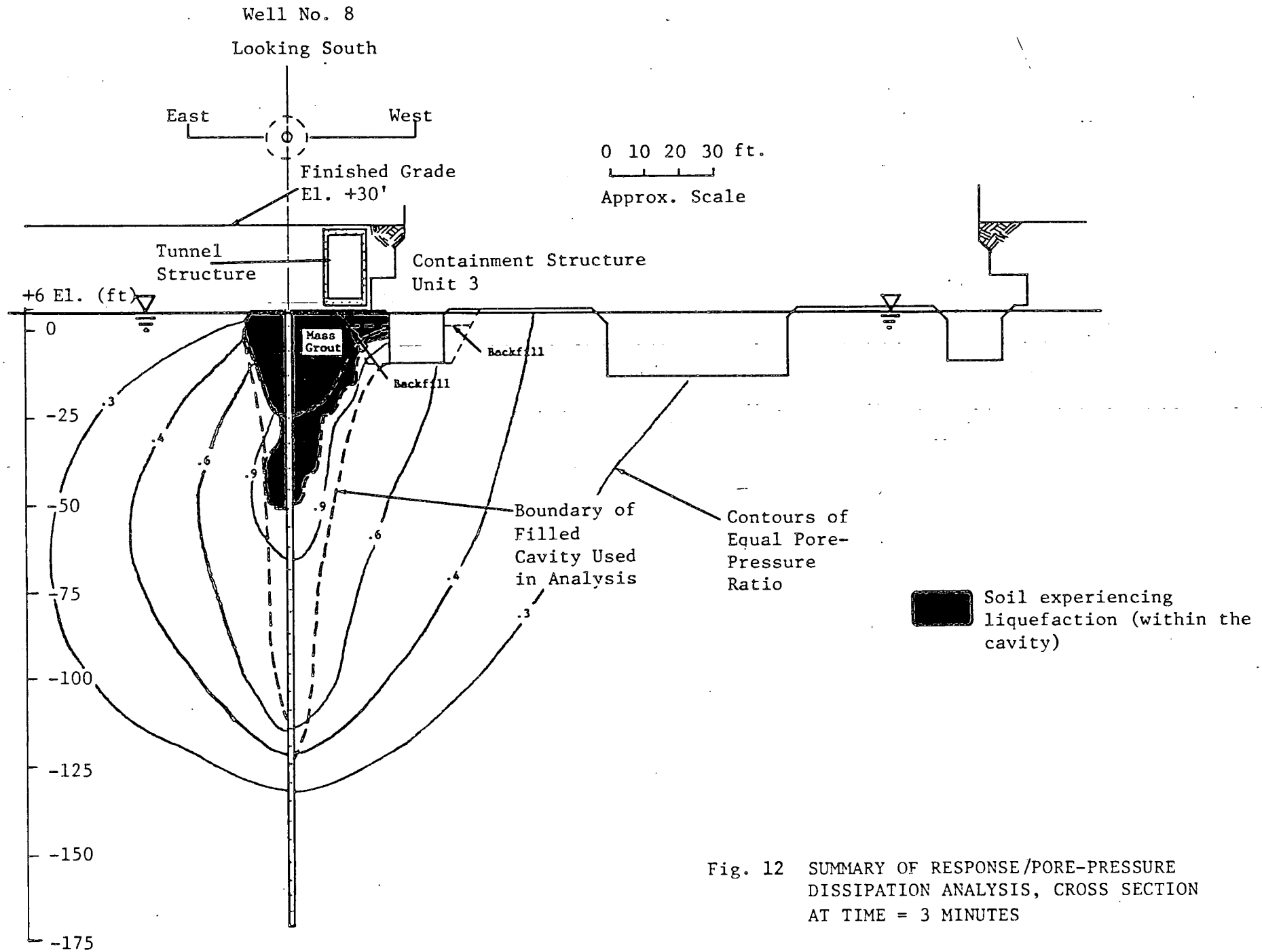

Fig. 12 SUMMARY OF RESPONSE/PORE-PRESSURE DISSIPATION ANALYSIS, CROSS SECTION AT TIME = 3 MINUTES

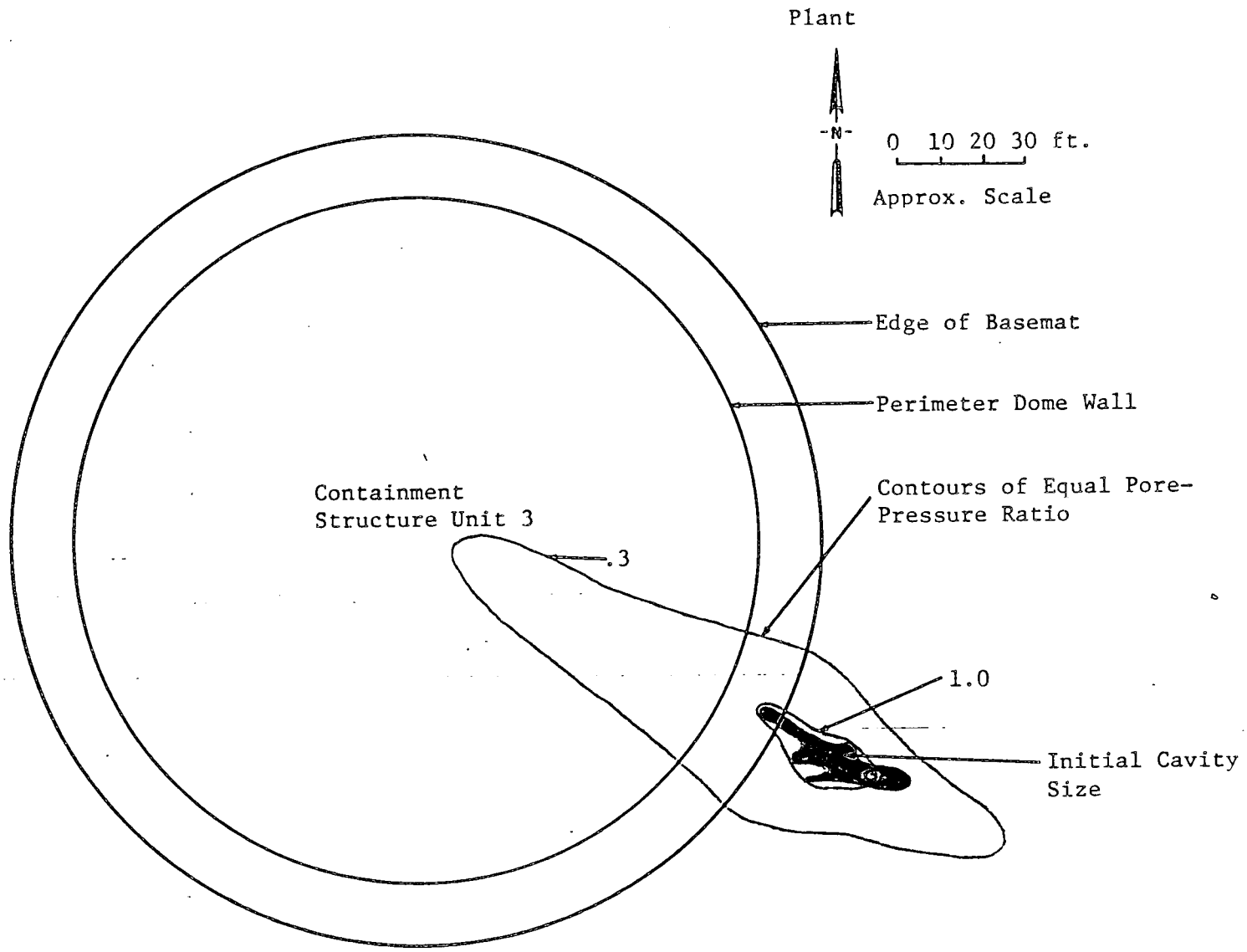

Fig. 13 SUMMARY OF RESULTS OF RESPONSE/PORE-PRESSURE ANALYSIS - FOR THE BASE OF TENDON GALLERY AT TIME = 3 MINUTES

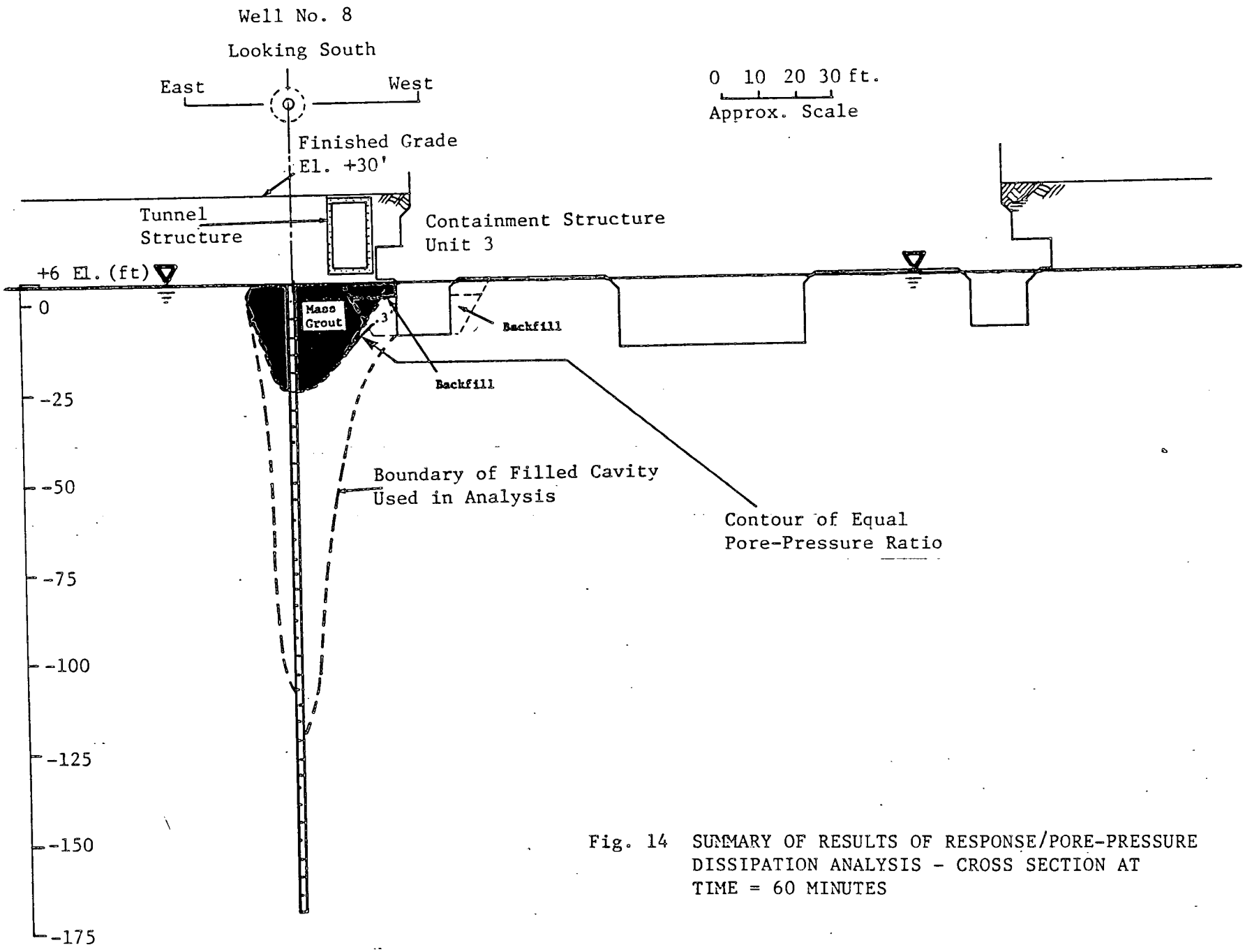

Fig. 14 SUMMARY OF RESULTS OF RESPONSE/PORE-PRESSURE DISSIPATION ANALYSIS - CROSS SECTION AT TIME = 60 MINUTES

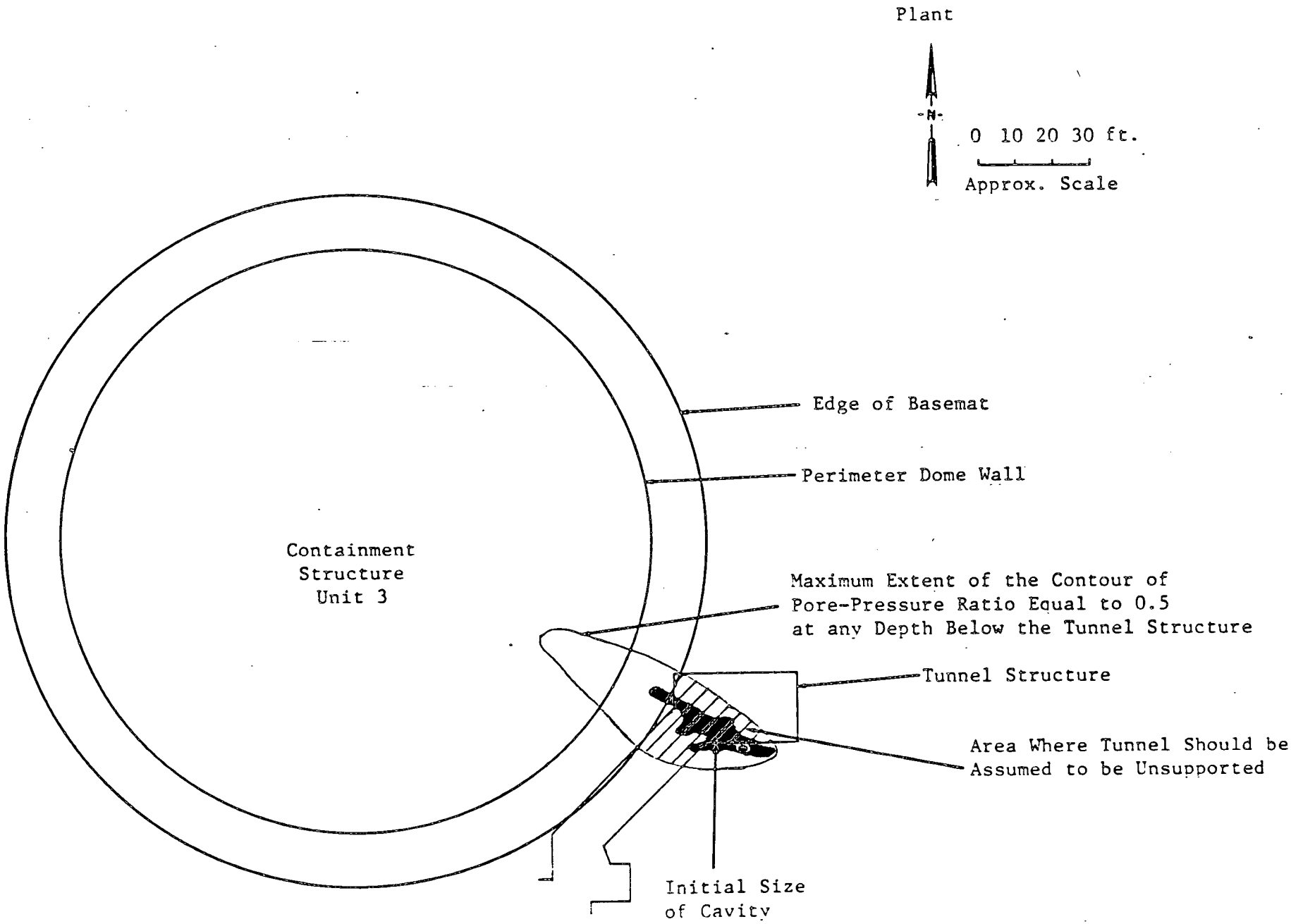

Fig. 15 MAXIMUM INTERPRETED EFFECT OF THE CAVITY ON THE TUNNEL STRUCTURE

APPENDIX A
DYNAMIC MATERIAL PROPERTIES

A.1 GENERAL

For the dynamic response computations, dynamic material properties must be assigned to the native San Mateo Sand, the cavity fill sand in the vicinity of Well 8, the grout, the tunnel immediately above the grout and the Unit 3 containment structure. The properties of greatest significance are shear modulus and damping ratio including their variations with strain. For this study, the dynamic properties were assigned based on the data documented in Appendix 2.5D of the FSAR for the project and published data for similar materials. Other properties required for the response computations are total unit weight and Poisson's ratio.

A.2 DYNAMIC PROPERTIES OF SAN MATEO SAND

A.2.1 Shear Modulus

The shear modulus of the native San Mateo Sand and fill has been shown to be dependent on the effective mean normal stress. The relationship between the shear modulus at very low strains, G_{max}, and the effective normal stress, $\bar{\sigma}_m$, for the native San Mateo Sand and fill can be represented by:

$$G_{max} = 59\ (\bar{\sigma}_m)^{2/3}\ \text{ksf}$$

where $\bar{\sigma}_m$ is in psf.

For purposes of analysis and in the interest of conservatism the cavity fill sand surrounding Well 8 has been estimated to have a relative density varying from approximately 30 to 50%. Based on data by Seed and Idriss (1970), the relationship between G_{max} and $\bar{\sigma}_m$ for the cavity fill sand was estimated to be:

$$G_{max} = 34\ (\bar{\sigma}_m)^{1/2}\ ksf$$

where $\bar{\sigma}_m$ is in psf.

The effective mean normal stress, σ_m, is defined by:

$$\bar{\sigma}_m = \left(\frac{1 + 2\ K_o}{3}\right)\ \sigma_v$$

where K_o = coefficient of lateral earth pressure at rest

σ_v = effective vertical stress

The value of K_o for the native San Mateo Sand, fill and cavity fill sand was estimated to be 0.35. Reasonable variations of this parameter would have only minor effects on modulus values.

The variations of shear modulus with strain utilized in response computations are shown in Figures 3 and 4 for the native San Mateo Sand and fill, and the cavity fill sand, respectively. The relationship shown in Figure 3 was developed previously for the project, based on laboratory test data of the native San Mateo Sand and fill. Shown in Figure 4 for the cavity fill sand is the average relationship for sand, published by Seed and Idriss (1970).

A.2.2 Damping Ratio

The variations of damping ratio with strain used in response computations are shown in Figures 3 and 4 for the native San Mateo Sand and fill, and the cavity fill sand, respectively.

The relationship shown in Figure 3 for the native San Mateo Sand and fill was developed previously for the project, based on laboratory test data. The relationship shown in Figure 4 for the cavity fill sand is the average relationship for sand, published by Seed and Idriss (1970).

A.2.3 Other Parameters

The values of total unit weight, γ_t, and Poisson's ratio, μ, used in analyses are summarized in Table A-1.

A.3 CONTAINMENT STRUCTURE AND TUNNEL

The approximate geometries of the Unit 3 containment structure and the adjacent tunnel are shown in Figures 2a and 2b. The outside diameters of the containment shell and foundation mat are approximately 150 feet and 192 feet, respectively. The total weight of the Containment Building, excluding the foundation mat, is approximately 83,600 kips. The weight of the foundation mat is approximately 66,900 kips. The fundamental frequency of the superstructure of the Containment Building is approximately 9.75 H_z during the horizontal excitation. The center of gravity of the superstructure is approximately 67 feet above the top of the foundation mat. Other parameters of the dynamic model in the E-W direction for the superstructure are summarized in Table A-2.

The average thickness of the foundation mat of the containment structure is approximately 14 feet. The value of compression modulus equal to 454,000 ksf and the value of Poisson's ratio equal to 0.2 are assumed. The value of damping ratio assumed is equal to 7%.

As shown in Figures 2a and 2b, the tunnel adjacent to the Unit 3 containment structure is 12 feet wide and 22 feet high. The thickness of the tunnel wall is approximately 1 foot and the thickness of the foundation is approximately 2 feet. The total pressure of the tunnel is approximately 1.87 ksf. A reasonable value of compression modulus equal to 454,000 ksf and a value of Poisson's ratio equal to 0.2 are assumed. The value of damping ratio is assumed to be 7%.

A.4 GROUT

The geometry of the grout is shown in Figures 2a and 2b. The properties of the grout are assumed to be those of weak concrete. The unit weight of the grout is assumed to be 150 pcf. The value of compression modulus equal to 360,000 ksf and the value of Poisson's ratio equal to 0.2 are assumed.

Table A-1

SOIL PARAMETERS USED IN DYNAMIC RESPONSE ANALYSES

Material	Unit Weight (pcf) Moist	Unit Weight (pcf) Saturated	K_o (a)	Poisson's Ratio μ	Maximum Shear Modulus Parameters (b) K_{max}	Maximum Shear Modulus Parameters (b) n	Variation of Shear Modulus G/G_{max}	Damping Ratio λ
Native San Mateo Sand and Fill	130	138	0.35	0.33	59	0.67	(c)	(c)
Cavity Fill Sand	--	120	0.35	0.33	34	0.5	(d)	(d)

(a) K_o = Ratio of horizontal effective stress to vertical effective stress

(b) $G_{max} = K_{max} (\bar{\sigma}_m)^n$

(c) As shown in Figure 3

(d) As shown in Figure 4

Table A-2

PROPERTIES OF DYNAMIC MODEL IN E-W DIRECTION FOR THE CONTAINMENT BUILDING

Width of Structure	160 ft
Compression Modulus (E)	524,000 ksf
Poisson's Ratio (μ)	0.2
Damping Ratio (λ)	7%
Area	3,956 ft^2
Shear Area	2,293 ft^2
Moment of Inertia (I)	466,717 ft^4
Weight*	83,600 kips

* Mass specified at mass point 67 ft above the top of the foundation mat.

APPENDIX B
CYCLIC STRENGTH CHARACTERISTICS OF SAN MATEO SAND

B.1 CYCLIC STRENGTH CHARACTERISTICS OF NATIVE SAN MATEO SAND

The foundation soil beneath the containment structure and other structures is the San Mateo Formation. This formation extends to approximately elevation -850 feet. As described in Section 2.5.4.2.1.3 of the FSAR for the project, this formation consists of a dense to very dense, well graded sand with apparent cohesion. The cyclic strength characteristics of the native San Mateo Sand were assessed, based on results of laboratory cyclic test data described in previous reports. Figure B-1 summarizes the variations of cyclic stress ratio ($\sigma_d/2\sigma_{3c}$) with number of stress cycle (N) for confining pressures ranging from 500 to 4000 psf for the native San Mateo Sand. These data are for a condition of initial liquefaction (excess pore water pressure equal to confining pressure). The development of initial liquefaction does not necessarily imply that significant deformations or softening of the soil would occur. Recent studies by DeAlba, Chan and Seed (1975), Casagrande (1976), and Seed (1976) indicate that deposits with relative densities greater than 80% would have very low strain potential (less than approximately 6%) under cyclic loading conditions at moderate confining pressures, even if they developed a condition of initial liquefaction.

The data shown in Figure B-1 were used in conjunction with time histories of dynamic shear stress to compute equivalent uniform stresses and numbers of uniform cyclic stress required to cause initial liquefaction, described in Appendix D.

B.2 CYCLIC STRENGTH CHARACTERISTICS OF CAVITY FILL SAND

Recent field exploration data indicate that relative densities of

the cavity fill sand in the vicinity of Well 8 varied widely in the range of loose to dense. For this study, it was assumed in the analyses of excess pore water pressure generation and dissipation described in Appendix D that the cavity fill sand would liquefy approximately 6 seconds after the earthquake excitation. This is consistent with assuming a relative density of 30 to 50% (the low end of the loose to dense classification).

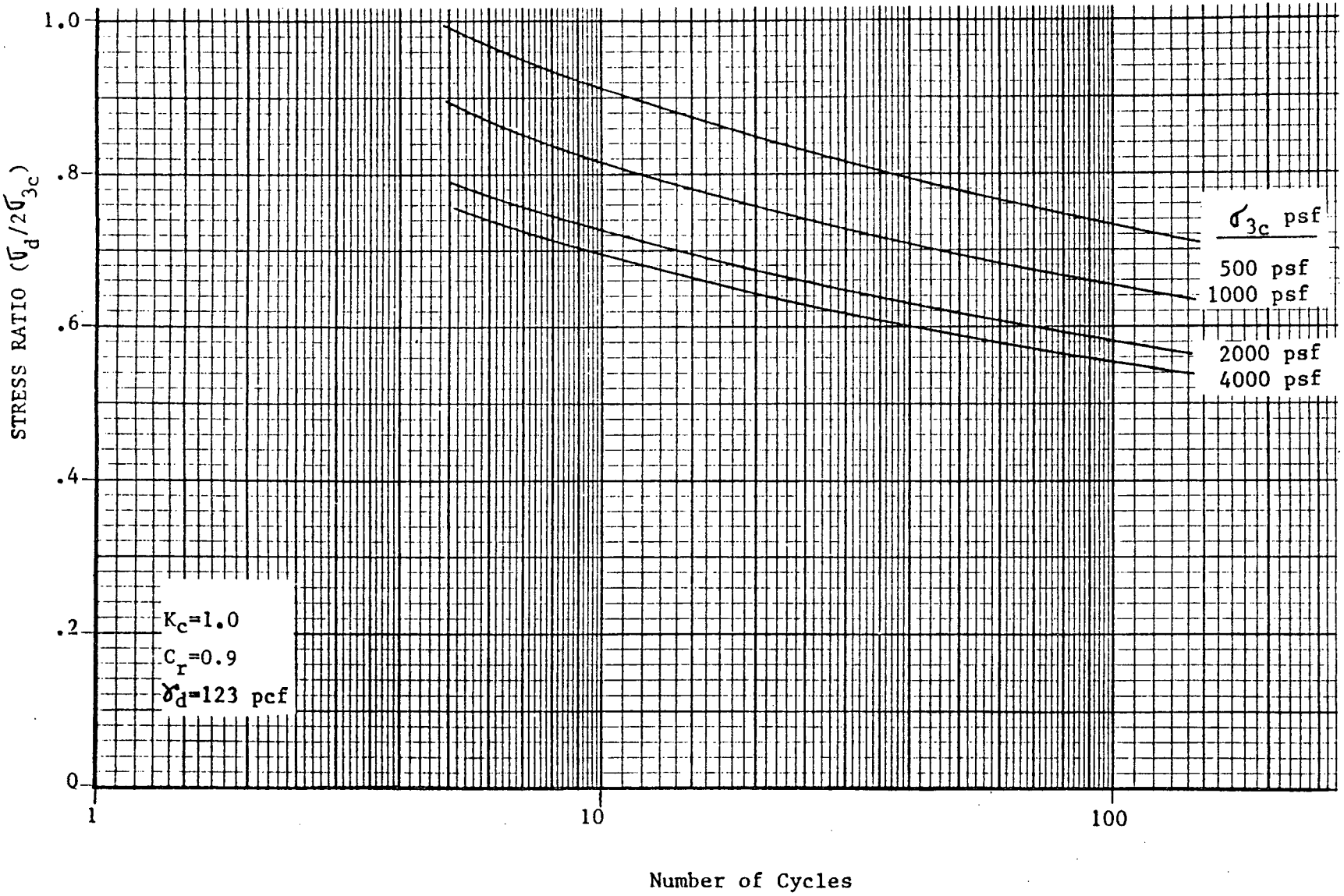

IN-SITU DYNAMIC STRENGTH OF SAN MATEO SAND

Fig. B-1

APPENDIX C
DYNAMIC RESPONSE ANALYSES

C.1 FREE-FIELD ONE-DIMENSIONAL RESPONSE ANALYSES

C.1.1 General

In conjunction with dynamic soil-structure interaction analyses, described subsequently in this appendix, a series of one-dimensional free-field response analyses, due to the postulated DBE, were made. Purposes of these analyses are (1) to provide a basis of checking the accuracy of two-dimensional dynamic finite element analyses and (2) to obtain the input base motion to the two-dimensional finite element model.

The basic analyses were conducted using the computer program SHAKE (Schnabel et al, 1972). The program FLUSH (Lysmer et al, 1975) was also used.

C.1.2 General Procedure

The one-dimensional free-field analyses were made using an equivalent linear method. The program SHAKE determines the response of a horizontally layered, linear viscoelastic system to an input earthquake motion by the method of wave propagation. Each soil layer is assumed to consist of a homogeneous isotropic material having thickness h, mass density γ, shear modulus G, and damping ratio λ. The input earthquake motion in the time domain is transformed into the frequency domain and transfer functions are analytically determined for each soil layered in the viscoelastic continuum. The transfer functions and input earthquake motion are combined in the frequency domain and then transformed to the time domain. The strain dependent nature of the shear modulus and damping in soils is accounted for by the use of equivalent linear soil properties using an iterative

procedure to obtain values of modulus and damping that are compatible with the effective strains in each soil layer.

C.1.3 Input Motion

The artificial time history of acceleration representing the postulated DBE previously developed for the project was used as the control motion for the response computations. The control motion is specified at the finished grade (Elevation +30 feet) of the plant site. The original accelerogram with a total duration of approximately 80 seconds has a peak acceleration of 2/3g and is digitized at 0.01 seconds. To reduce the computer core size required for response analyses, it is desirable to redigitize at a time increment of 0.04 seconds. This was performed using an option in SHAKE. Figure C-1 shows the comparison of the original and redigitized accelerograms. The effects of using the redigitized accelerogram in the response computations are examined subsequently in the one-dimensional free-field analyses.

C.1.4 Results of One-Dimensional Analyses

A series of one-dimensional analyses were performed using the programs SHAKE, and FLUSH. Comparisons of responses from FLUSH with those from SHAKE would provide a basis for evaluating adequacy of element sizes and use of the redigitized control motion (Δt = 0.04 seconds).

Comparisons of values of peak shear stress obtained from the SHAKE analyses using the control motion digitized at time increments of 0.02 and 0.04 seconds are shown in Figure C-2. Figure C-2 indicates that the peak shear stresses obtained from response analyses using the control motion digitized at 0.02 and 0.04 seconds are practically identical. It is concluded that response analyses using the control motion digitized at Δt = 0.04 seconds should provide reasonably accurate computations of shear stresses.

Figure C-3 compares values of peak shear stress obtained from SHAKE and FLUSH analyses. The results indicate that the FLUSH analysis gives practically identical stresses to those from the SHAKE analysis. Based on these results, it can be concluded that the element sizes selected for the response analyses, using the FLUSH program, are adequate and use of the control motion digitized at $\Delta t = 0.04$ seconds is sufficient for stress computations.

C.2 DYNAMIC RESPONSE ANALYSES OF SOIL-STRUCTURE SYSTEM

C.2.1 General

Analysis of potential for cyclic straining and excess pore water pressure generation of the San Mateo Sand beneath the containment structure and surrounding the Well 8 cavity requires time histories of induced shear stresses due to the DBE. The induced shear stresses can be computed from dynamic response analyses of a soil-structure system incorporating the containment structure, the tunnel structure, the grout and the soil fill within the cavity at Well 8. The response analysis was made using the computer program FLUSH (Lysmer et al, 1976).

C.2.2 General Method of Approach

The soil-structure interaction studies were made using the finite element method (Idriss et al, 1973; Lysmer et al, 1975) in which soil and structures were modeled in a combined system. The general method of approach used involves the following main steps:

1. The control motion was specified at the finished grade in the free-field.

2. Using deconvolution analyses, a motion was computed at the base of the soil-structure model. The base motion is the motion that would have to develop at the base of the model in order to produce the specified free-field control motion.

3. The base motion obtained in Step 2 was then used as excitation to the soil-structure finite element model. The dynamic analysis of the model allows the response including stress and acceleration time histories to be computed at any selected points in the system.

For this study, the dynamic response of the soil-structure system was evaluated using the computer program FLUSH. The FLUSH program incorporates the equivalent linear method described by Idriss et al (1969) to simulate nonlinear soil behavior. The advantages of using the FLUSH program include the following:

1. A three-dimensional approximation of soil-structure interaction effects. This is accomplished by using energy-absorbing viscous dashpots to provide radiation damping in the third direction, i.e., these dashpots remove energy radiating in the third direction.

2. Use of transmitting boundaries which greatly reduce the number of elements required to minimize boundary effects, thus allowing for the use of a finer element mesh in the area of interest (in this case the area of the cavity at Well 8 and the Unit 3 containment) while sill remaining within the core capacity of the computer.

C.2.3 Finite Element Model

The finite element soil-structure model used in the FLUSH analyses is shown in Figure 5. This model corresponds to the maximum vertical section of the filled cavity projected to a plane through Well 8 and the center of the Unit 3 containment structure. The model incorporates the Unit 3 containment structure, the tunnel structure, the grout and the soil filled cavity. Subsequent field exploration data presented in the Well 8 field investigation report indicated that the actual shape of the cavity may be slightly different from that used in the

model. However, because the size of the cavity assumed in the model is extremely conservative, any minor variations in the shape of the cavity are expected to have insignificant effects on the response computations. The containment structure is idealized by a stick model located at the centerline of the structure. The model parameters are described in Appendix A. The spatial effects of the dynamic response of the stick models on the structural response of the total system are incorporated through the use of an outrigger beam at the top of the foundation mat.

The model conservatively assumed the axis of the containment structure to be the axis of symmetry; thus, assuming cavities on both sides of the containment structure. A transmitting boundary is provided at the left side of the model. Viscous dashpots are provided for the foundation mat to absorb energy radiating in the third direction. The width of the model is conservatively assumed to be 25 feet corresponding to the maximum width of the cavity (see Figure 2a).

C.2.4 Analysis Results

Results of dynamic analyses include time histories of acceleration and stress at selected locations in the soil-structure system.

Typical time histories of induced shear stress computed near the sand-filled cavity are shown in Figure C-4. Variations of peak shear stress along two selected horizontal sections (elevations -22.5 and -46 feet) are shown in Figure C-5. The time histories of induced shear stress were converted to equivalent uniform stresses for each element and used to define excess pore water pressure generation characteristics described in Appendix D.

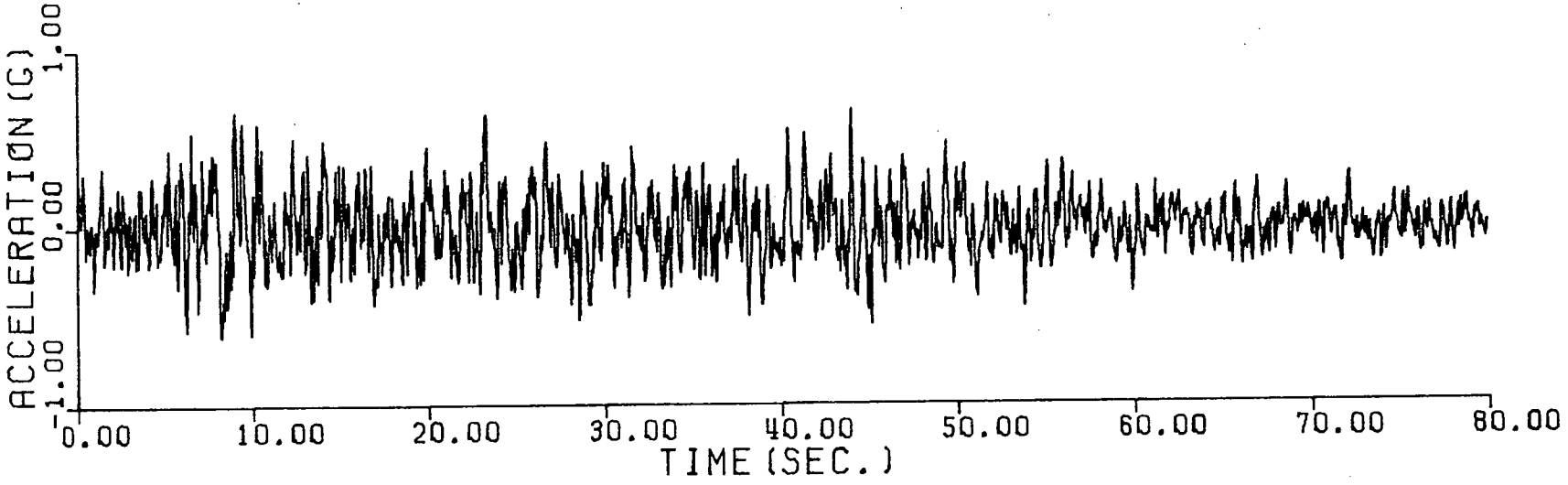

(a) Δt = 0.04 secs.

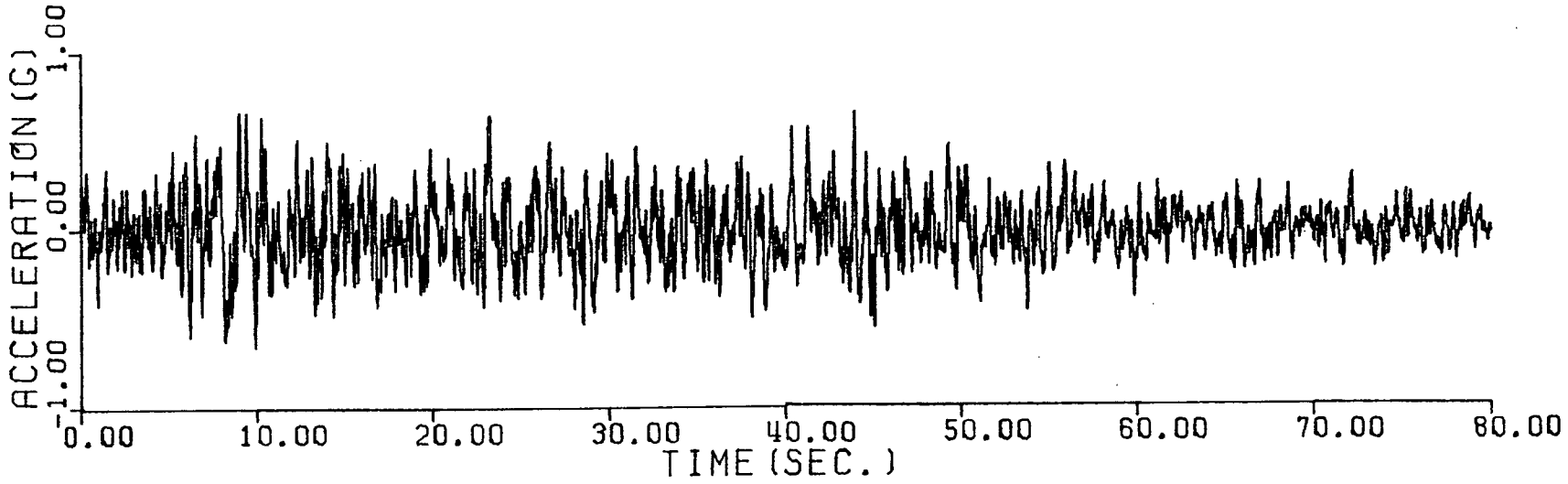

(b) Δt = 0.01 secs.

FIG. C-1 TIME HISTORIES OF ACCELERATION REPRESENTING THE DBE FOR DIGITIZATION TIMES OF Δt = 0.04 AND 0.01 SECS.

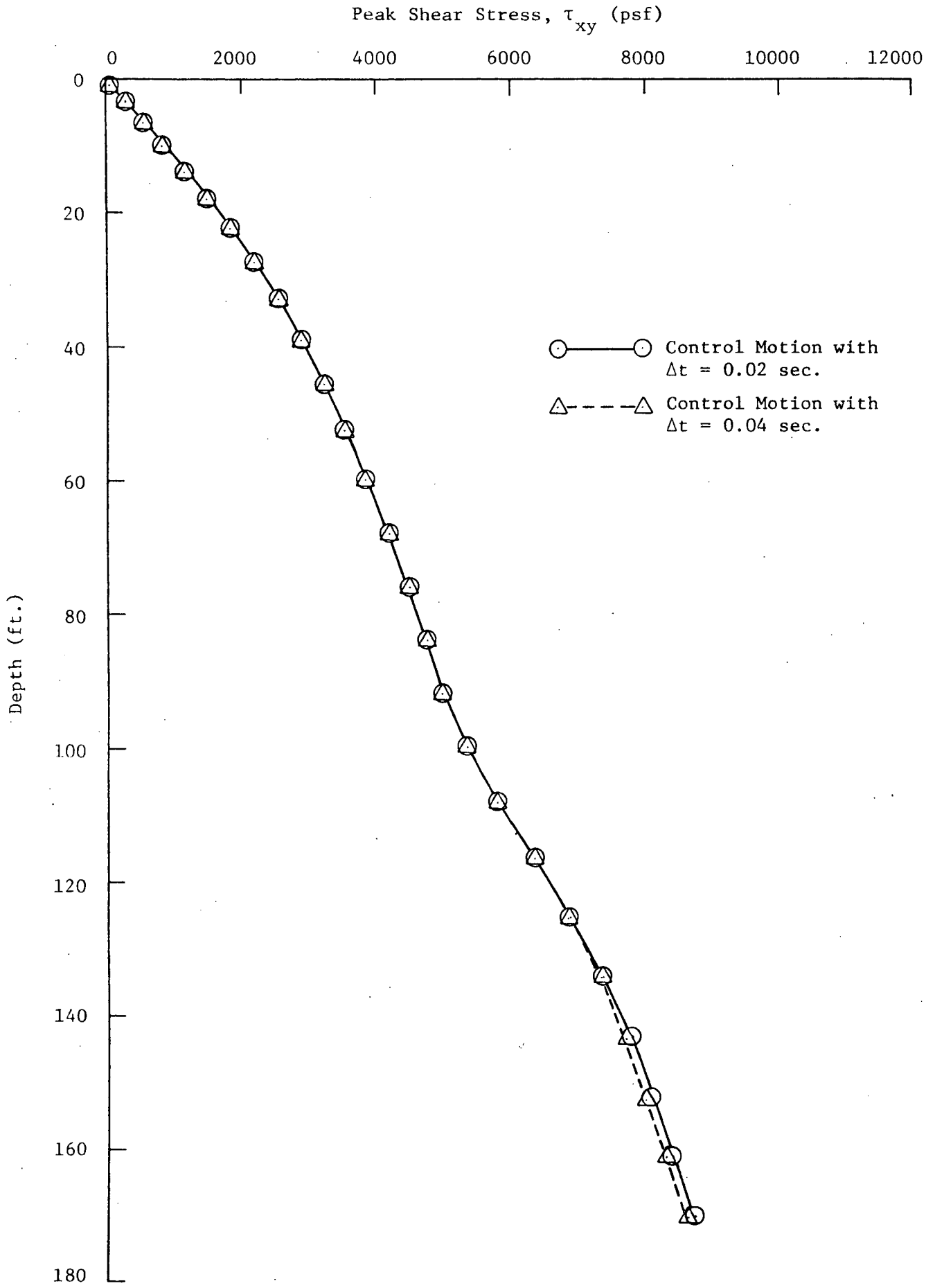

Fig. C-2 COMPARISONS OF PEAK SHEAR STRESSES FROM SHAKE ANALYSES USING DBE CONTROL MOTION WITH Δt = 0.02 and 0.04 SECOND

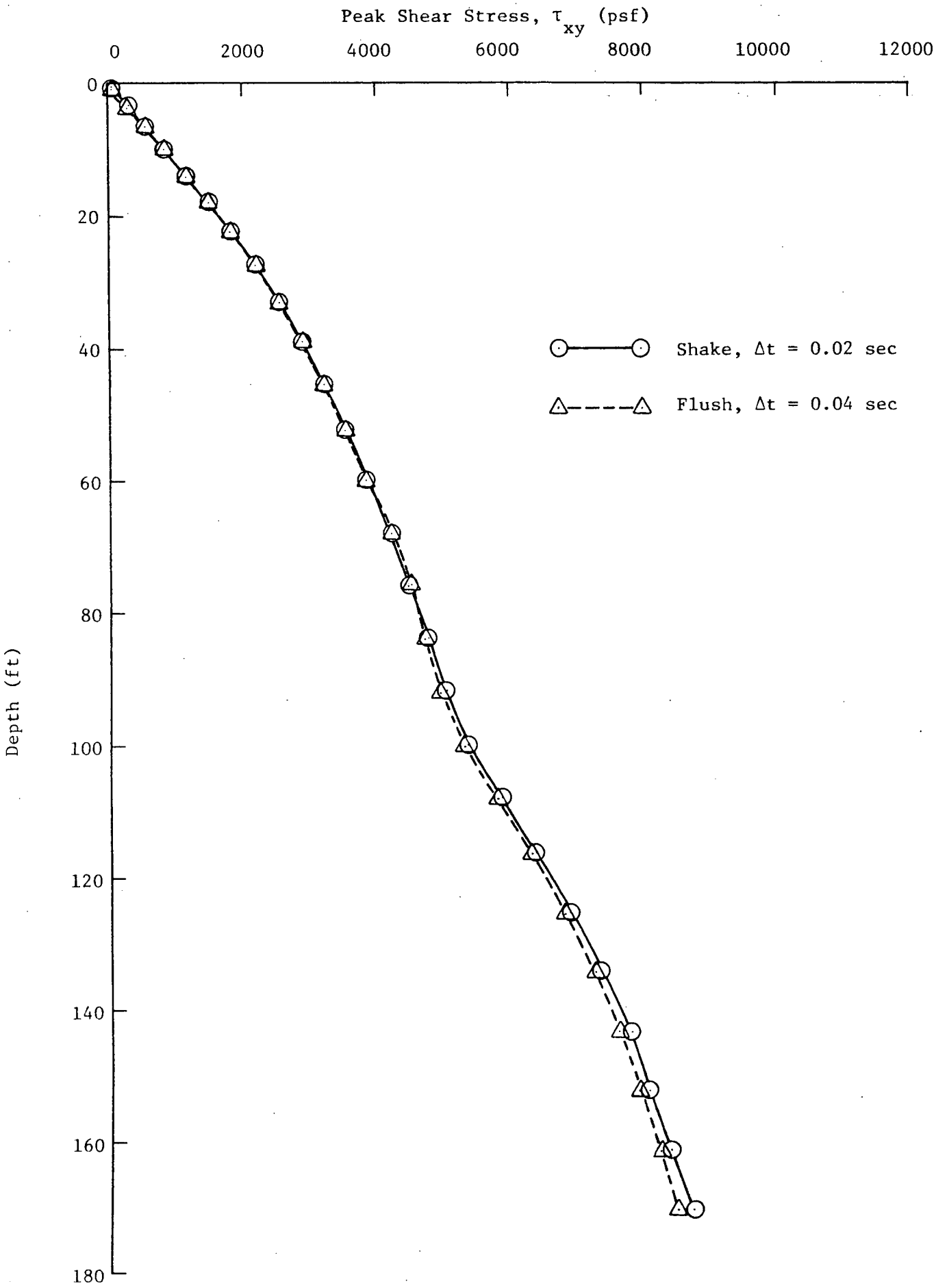

Fig. C-3 COMPARISON OF PEAK SHEAR STRESSES FROM SHAKE AND FLUSH FREE-FIELD ANALYSES

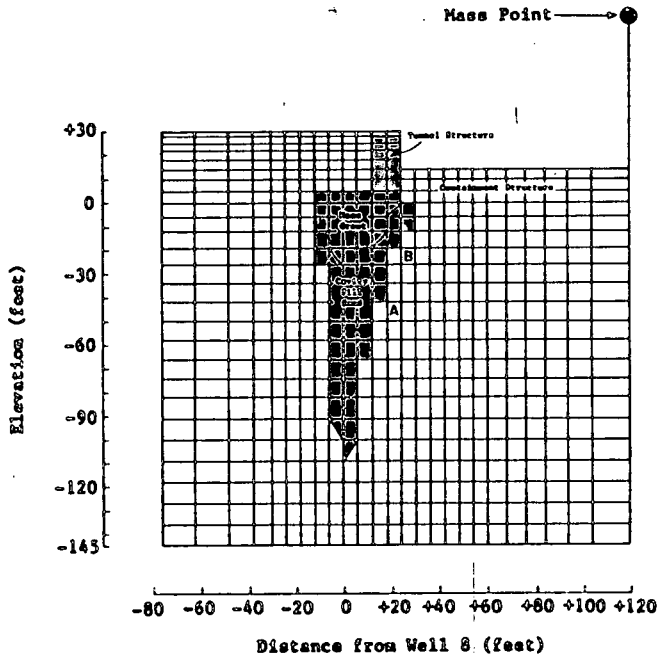

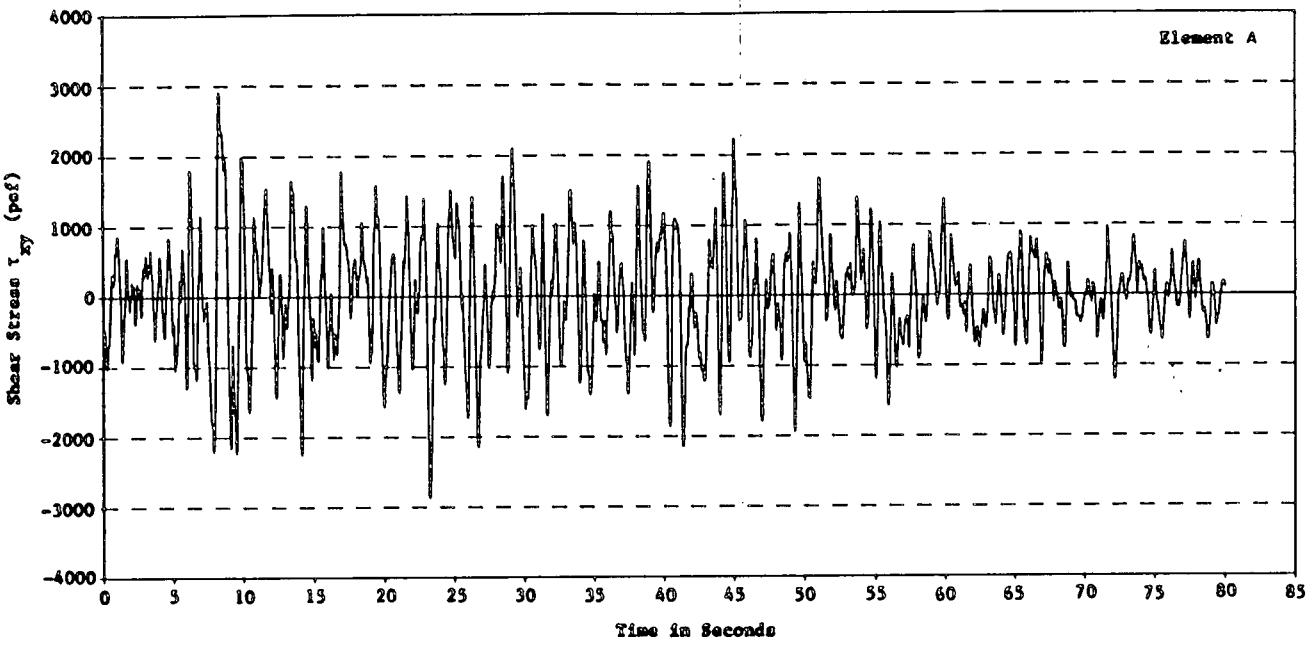

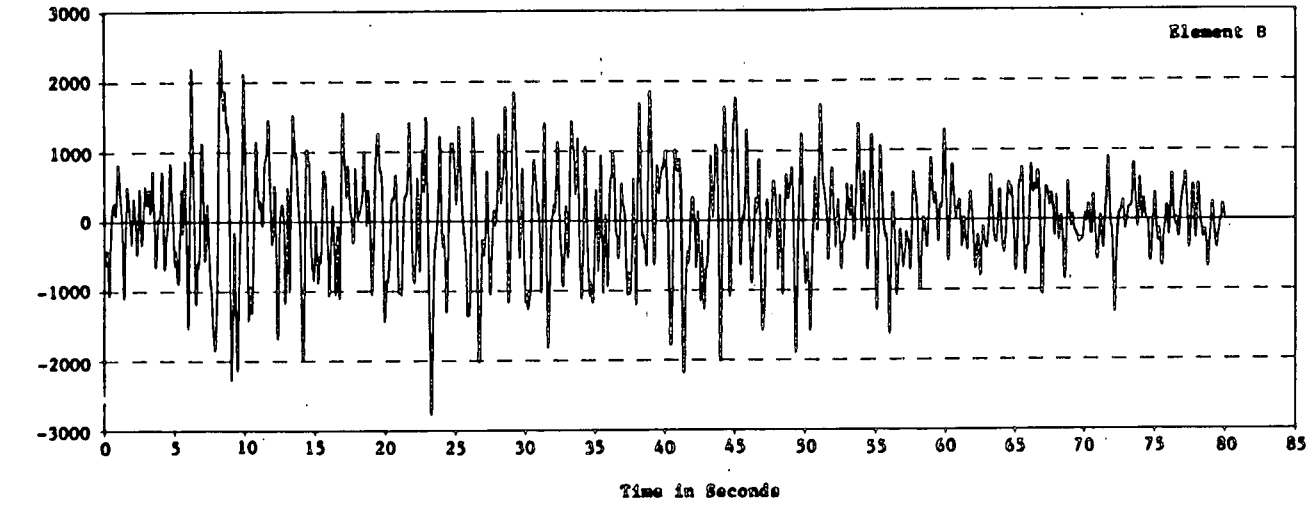

Fig. C-4 TYPICAL TIME HISTORIES OF SHEAR STRESSES AT SELECTED ELEMENTS

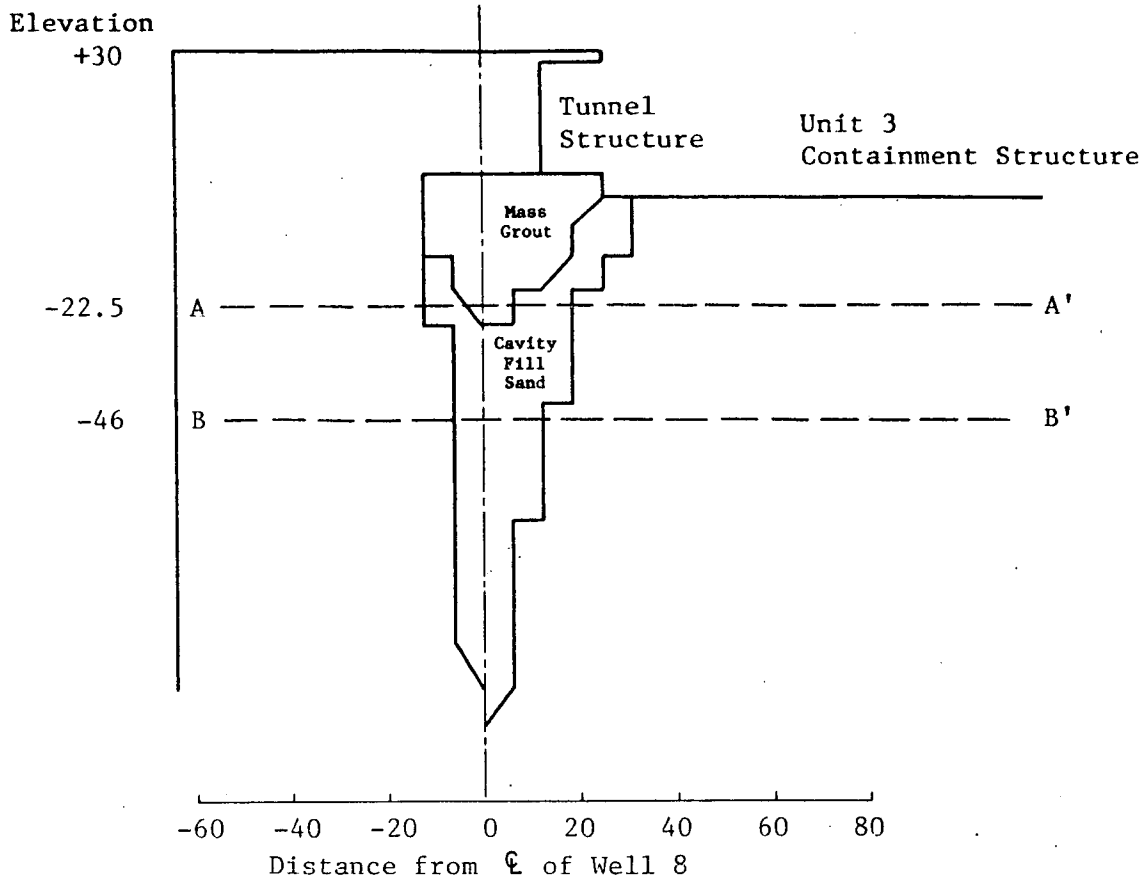

Section AA'

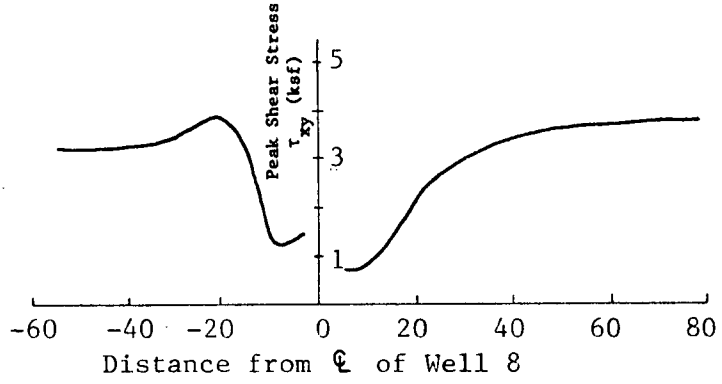

Section BB'

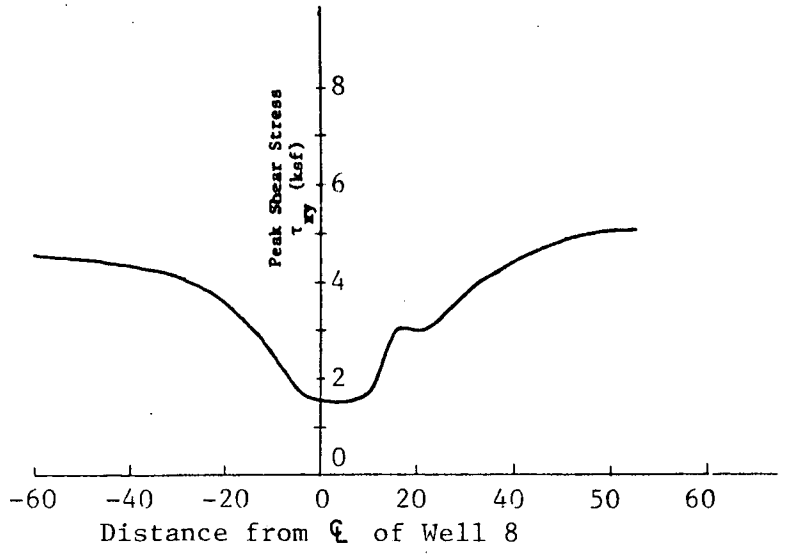

Fig. C-5 DISTRIBUTION OF PEAK SHEER STRESS THROUGH TYPICAL SECTIONS DUE TO DBE

APPENDIX D
ANALYSES OF EXCESS PORE WATER PRESSURE GENERATION AND DISSIPATION

D.1 INTRODUCTION

The seismic shaking of a granular soil deposit below the water table produces cyclic shear stresses which under undrained conditions will cause an increase in pore water pressures. The increase in pore water pressures will in turn affect the load carrying capacity of each individual soil element and may lead to excessive cyclic straining within the soil deposit. During the last decade, analysis of the liquefaction and excessive cyclic straining potential due to seismic shaking has been based on undrained conditions in which the effects of the redistribution and dissipation of pore pressures on the liquefaction potential of the soil mass were assumed to be insignificant.

Recently, analysis techniques have been developed to couple both generation and dissipation of pore water pressures in the evaluation of the liquefaction potential of the soil mass during and after seismic shaking. The analysis techniques include those developed by Seed, Martin and Lysmer (1975) for one-dimensional conditions and by Seed and Booker (1976), Rahman, Seed, and Booker (1976) and Booker, Rahman, and Seed (1976) for two-dimensional plane strain or axisymmetric problems. These techniques were employed in this study to evaluate generation and dissipation of excess pore water pressures in the native San Mateo sand formation surrounding the soil filled cavity at Well 8. The following sections briefly describe the general procedures of analysis, parameter selections, analysis models and analysis results.

D.2 GENERAL PROCEDURES OF ANALYSIS

General procedures for analysis of pore pressure generation and

dissipation involve the following steps:

1. Determine or estimate, based on published data for similar soil deposits, the permeability and volume compressibility of the soil mass. Consider variations of these parameters with both relative density and pore pressure ratio (r_u, ratio of pore water pressure to mean bulk effective stress or vertical effective stress).

2. Determine the cyclic strength and pore water pressure generation characteristics of the soils subjected to cyclic loading under undrained conditions.

3. Convert time histories of induced dynamic shear stress with varying amplitudes to an equivalent number of cycles with a uniform cyclic stress for each element in the soil mass. The induced cyclic stresses together with data obtained in Step 2 are then used to prescribe the source pore water pressure generation during seismic shaking for each soil element.

4. Represent the actual field conditions by finite element models with appropriate boundary conditions.

5. Formulate and solve the equations governing pore pressure generation and dissipation by numerical techniques.

The computer program GADFLEA following the above procedures was developed by Booker, Rahman, and Seed (1976). This program was used in this study.

D.3 PARAMETER SELECTIONS

D.3.1 Permeability and Volume Compressibility of San Mateo Sand

The grain size characteristics, permeability and coefficients of volume compressibility of San Mateo Sand (native San Mateo

formation and sand fill within the cavity) were selected on the basis of laboratory and field test data previously developed for the project, and published data for similar materials. These data are summarized in Table D-1.

The permeability (K_H and K_v) and the coefficient of volume compressibility (m_{vo}) of the grout within the cavity were assumed to be very small ($K_H = K_v = 5 \times 10^{-5}$ cm/sec; $m_{vo} = 1 \times 10^{-7}$ ft^2/lb) compared to those of the native San Mateo Sand.

In the analysis of pore pressure generation and dissipation, the coefficients of permeability were generation and dissipation, the coefficients of permeability were assumed constant (Seed, Martin, and Lysmer, 1975). However, Seed, Martin, and Lysmer (1975) found that the values of compressibility (m_v) are influenced by both relative density and pore pressure ratio when pore pressure ratios are higher than about 60%. The variation of m_v with these two variables was found to be approximated by the relationship:

$$\frac{m_v}{m_{vo}} = \frac{e^y}{1 + y + (1/2)\, y^2} \qquad \text{(D-1)}$$

where m_{vo} is the compressibilty for zero pore pressure ratio (r_u):

$$y = A\,(r_u)^B$$
$$A = 5\,(1.5 - D_r)$$
$$B = 3\,(2)^{-2D_r}$$

and D_r is the relative density.

As described previously, the native San Mateo Sand is very dense and was assumed $D_r = 1.0$ in the analysis. The soil fill within the cavity was assumed to have $D_r = 0.3$.

D.3.2 Pore Pressure Generation Characteristics

The pore pressure generation characteristics define the rate of pore pressure generation (du_g/dt) for each element under undrained conditions due to seismic shaking. The parameter du_g/dt may be expressed in the form of:

$$\frac{du_g}{dt} = \frac{\partial u_g}{\partial N} \cdot \frac{\partial N}{\partial t} \qquad \text{(D-2)}$$

where

$\partial u_g/\partial N$ = the pore pressure generated by each cycle of alternating shear stress, and

$\partial N/\partial t$ = the rate of cycles of alternating shear stress.

For this study, $\partial N/\partial t$ was assumed equal to an average rate of cycles of alternating shear stress over a total duration of seismic shaking, i.e.:

$$\frac{\partial N}{\partial t} = \frac{N_{eq}}{t_d} \qquad \text{for } 0 < t < t_d \qquad \text{(D-3)}$$

and

$$\frac{\partial N}{\partial t} = 0 \qquad \text{for } t > t_d$$

where N_{eq} is an equivalent number of uniform cycles for the postulated earthquake and t_d is the duration of strong shaking. For the analyses conducted in this study, N_{eq} = 30 cycles was selected to represent the postulated DBE, and the value of t_d equals 80 seconds.

The value $\partial u_g/\partial N$ can be estimated from undrained cyclic tests. Booker, Rahman, and Seed (1976) shows that for many soils the

relationship between the pore pressure generated by the alternating shear stress, u_g, and cycles of alternating shear stress, N, may be expressed in the form of:

$$\frac{u_g}{\sigma_o'} = \frac{2}{\pi} \text{ arc sin } \left(\frac{N}{N_1}\right)^{\theta/2} \qquad \text{(D-4)}$$

where

N_1 = the number of cycles necessary to cause liquefaction.

σ_o' = the initial mean bulk effective stress for triaxial conditions or the initial vertical effective stress for simple shear conditions.

and θ = an empirical constant which depends on the soil type and test conditions.

For sands, values of θ typically varry from 0.7 to 1.0. For this study, θ was conservatively assumed equal to 1.0 resulting in a variation of u_g/σ_o' with N/N_1 shown in Figure D-1.

From Eq. D-4, the rate of pore pressure generation per cycle of uniform shear stress may be obtained as follows:

$$\frac{\partial u_g}{\partial N} = \frac{\sigma_o'}{\theta \pi N_1} \cdot \frac{1}{\sin^{2\theta-1} X \cos X} \qquad \text{(D-5)}$$

where $X = \frac{\pi}{2} r_u$

and $r_u = u/\sigma_o'$ the pore pressure ratio.

The values of N_1 were obtained from the cyclic strength data shown in Figure B-1 and the equivalent uniform cyclic stress for each soil element in the native San Mateo Sand formation. The values of equivalent uniform cyclic stress were obtained using the time histories of dynamic shear stress from the dynamic

response analysis described in Appendix C. The procedure for computing equivalent uniform cyclic stresses are similar to those described by Seed et al (1975).

The soil fill within the cavity was assumed to liquefy after three cycles of uniform stress applications, i.e., to liquefy in the early stage of seismic shaking (approximately 6 to 8 seconds after the beginning of seismic shaking).

D.4 ANALYSIS MODELS

In the analyses of pore water pressure generation and dissipation conducted for this study, both axisymmetric and plane strain finite element models were used. These models are shown in Figures D-2 and D-3 for the axisymmetric and plane strain models, respectively. An additional axisymmetric model with a cavity size more closely approximating the actual volume of the cavity at Well 8 (approximately 2-1/2 times the actual cavity volume as determined in the Well 8 field investigation report) was also analyzed. The basic analysis was made for the axisymmetric case to define pore water pressure redistribution beneath the Unit 3 containment structure. The plane strain solution was used as a basis to estimate pore water pressure redistribution in the direction away from the containment structure.

Both the basic axisymmetric and plane strain models were developed based on the geometry of the maximum cross-section of the cavity shown in Figure 2a. The axisymmetric model assumed that (1) the axis of symmetry is located at the center of Well 8; (2) the volume of the soil fill within the cavity is equal to the volume of revolution of a cross-section equal to the maximum section of the cavity; and (3) the model implies that the shortest drainage path is the one along the basemat of the containment structure, i.e., a drainage path equal to the diameter of the basemat. The plane strain model assumed that (1) the cavity is infinite in the third direction (i.e.,

perpendicular to the analysis section) and (2) the excess pore pressures can dissipate to both sides of the cavity (the shortest drainage path beneath the containment structure is still equal to the diameter of the basemat).

Both the models implied two very conservative assumptions with respect to excess pore water pressure generation and dissipation. These assumptions were: (1) the geometry of the sand fill within the cavity at Well 8 is two-dimensional (plane strain or axisymmetric) and (2) the shortest drainage path beneath the containment structure is equal to the diameter of the basemat. The first assumption implies that the volume of the pore pressure generating source is much greater than the actual size of the cavity. For the axisymmetric case which is considered to model the cavity size more realistically than that of the plane strain case, the volume of the cavity is calculated to be more than one order of magnitude larger than the actual cavity size. The effect of the assumed cavity volume on pore water pressure generation and dissipation is examined subsequently. The second assumption increases time required for dissipation of excess pore pressures and overestimates pore pressure at any given time during periods of dissipation as compared to the actual field condition. Figure 1 indicates that the bases of foundation mats for structures adjacent to Well 8 except the Unit 3 containment structure will be situated above the ground water table. Thus, any potential excess pore water pressures generated within the cavity should dissipate radially and quickly in the immediate vicinity of the well with drainage paths much shorter than those assumed in the analyses.

D.5 ANALYSIS RESULTS

The results of the pore water pressure generation and dissipation analyses conducted are summarized in Figures D-4 through D-9. These figures show the distributions of pore water pressure ratio (ratio of excess pore water pressure to effective vertical

stress) along the analysis section during and after the DBE seismic shaking (t = 12 seconds, 30 seconds, 80 seconds, 3 minutes, 30 minutes, and 60 minutes). The pore water pressure distributions under the Unit 3 containment structure were obtained from the basic axisymmetric case and those in the area away from the containment structure were estimated on the basis of the results from the plane strain and axisymmetric solutions.

The effects of using an axisymmetric model with a cavity size more closely approximating the actual volume of the cavity at Well 8 are illustrated in Figure D-10. Figure D-10 shows the comparisons of the distributions of pore water pressure ratio at t = 3 minutes obtained from the basic axisymmetric case based on the model with the maximum section of the cavity and the model more closely approximately the actual volume of the cavity. The comparisons indicate that the zone of high excess pore water pressures ($r_u > 0.3$) obtained from the model with the cavity more closely approximately the actual cavity volume is significantly smaller and shallower than the basic model used in this study.

The discussions of the analysis results and the use of these results in assessing the effects on the adjacent structures are presented in the main body of this report and in Appendix E.

Table D-1

Permeability and Volume Compressibility

of San Mateo Sand Used in Analysis

Material	D_{50} (mm)	Permeability* Coefficient (cm/sec) K_H	Permeability* Coefficient (cm/sec) K_V	Coefficient of Volume Compressibility** $m_{vo}(ft^2/lb)$
Native San Mateo Sand	.85 to 0.6	1.5×10^{-2}	10^{-2}	9×10^{-7}
Cavity Fill Sand	.85 to 0.6	6×10^{-3}	6×10^{-3}	1.8×10^{-6}

* The permeability coefficients of the native San Mateo sand were obtained based on the results of field permeability tests conducted previously for the project. The permeability of the soil fill within the cavity was selected from laboratory tests on reconstituted samples with dry density γ_d = 100 pcf.

** Based on data compiled by Martin (1975) using the original data by Lee and Albaisa (1974).

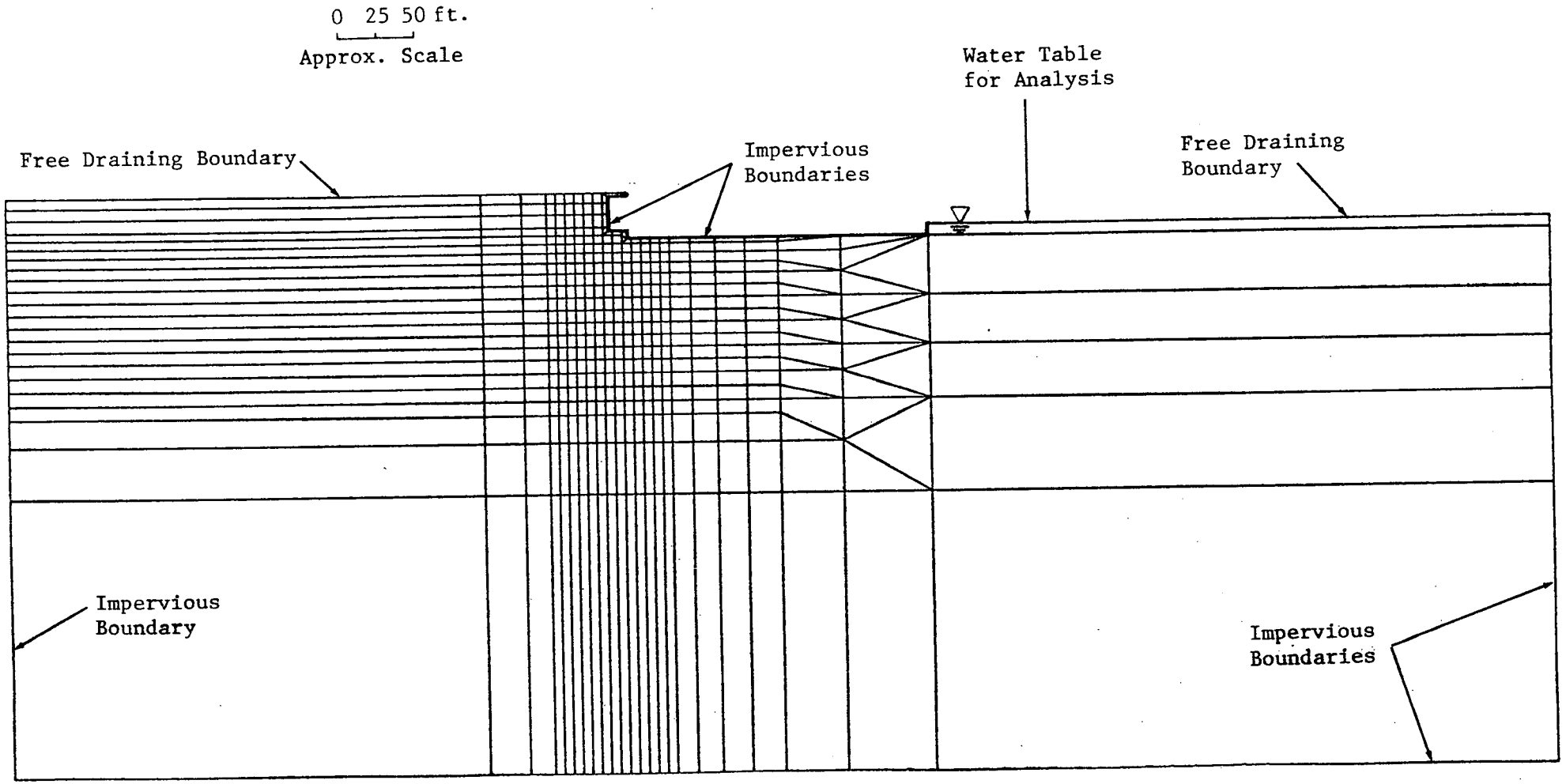

Fig. D-1 FINITE ELEMENT MESH FOR PLANE STRAIN ANALYSIS

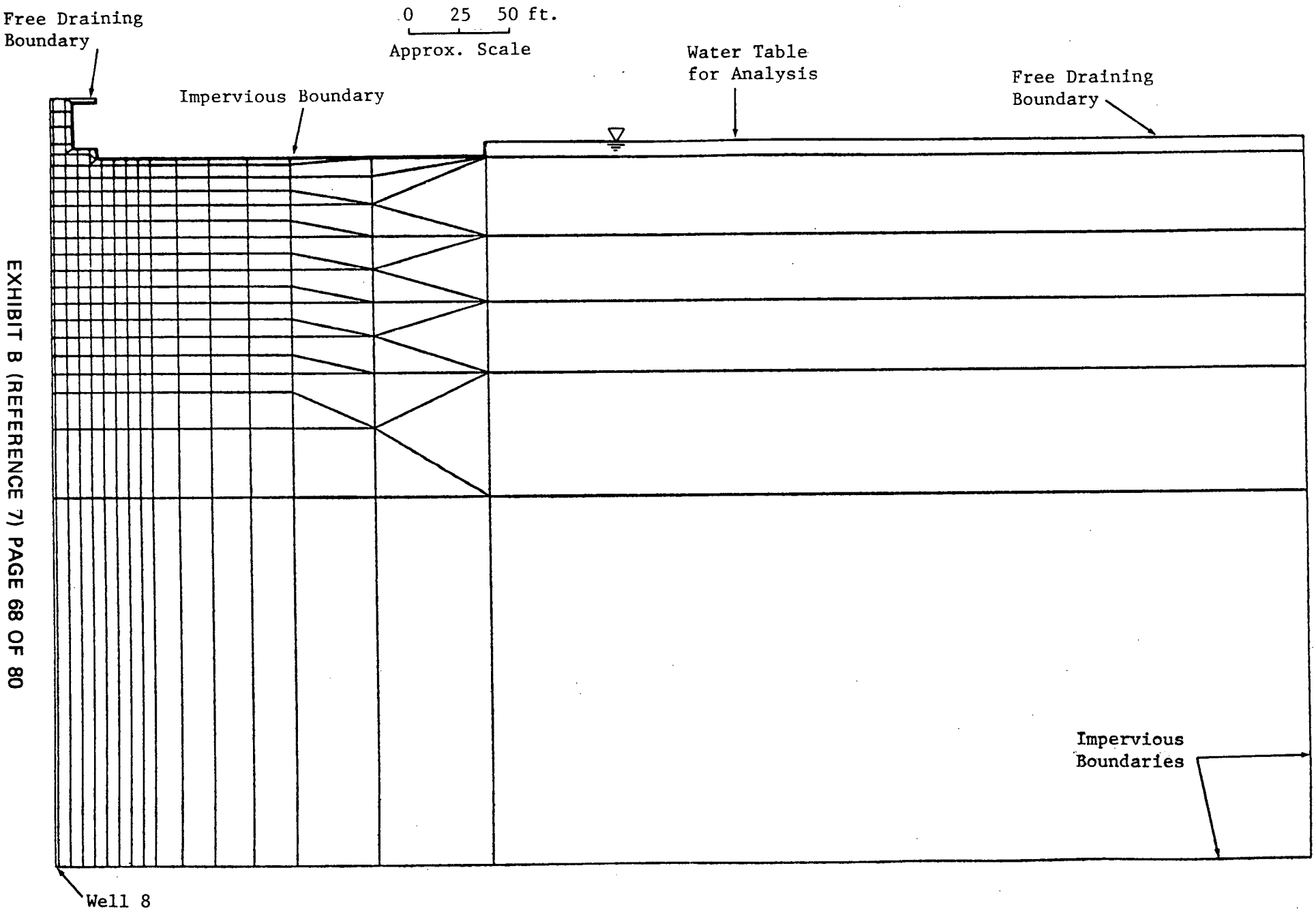

Fig. D-2 FINITE ELEMENT MESH FOR AXISYMMETRIC ANALYSIS

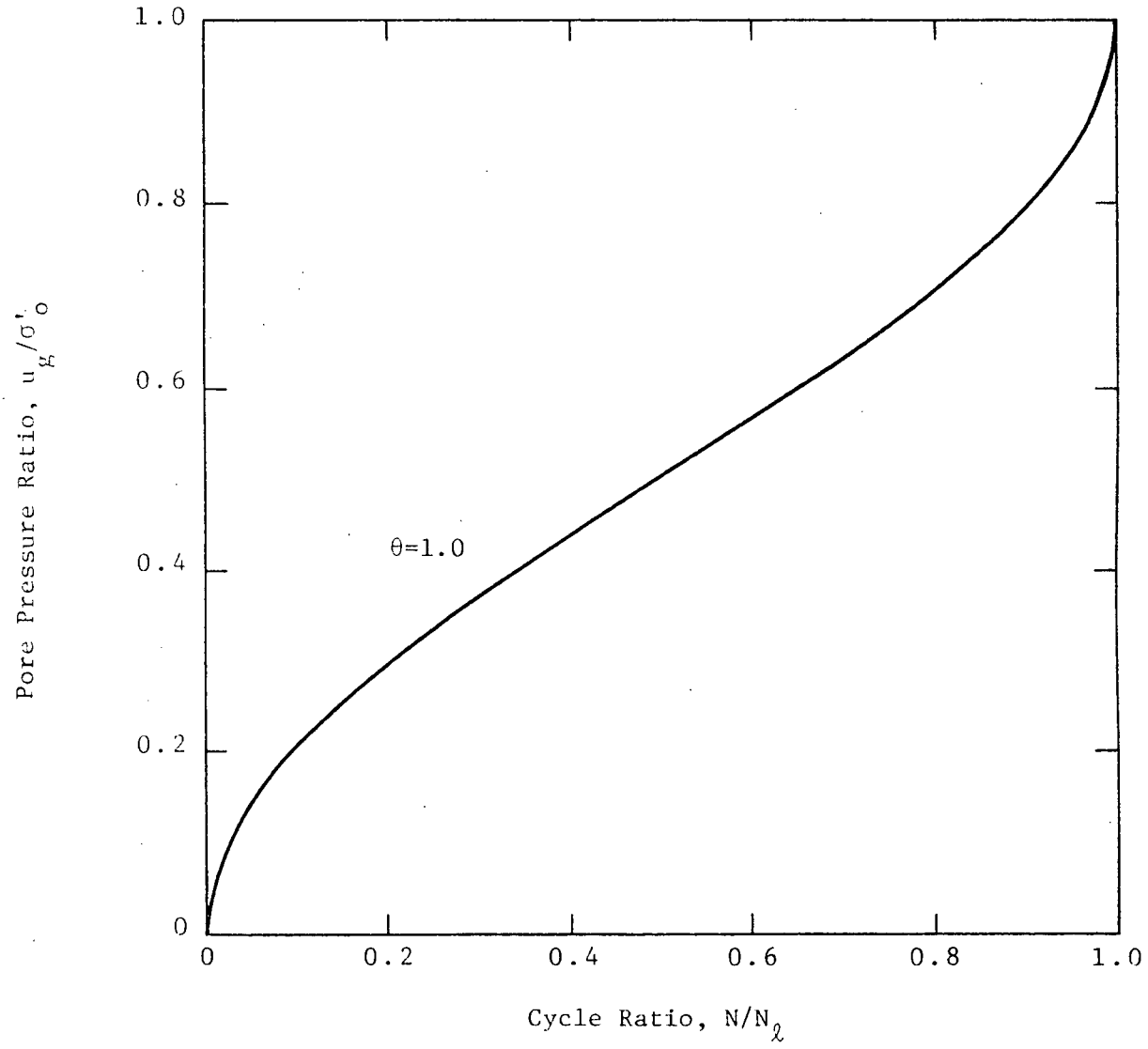

Fig. D-3 RATE OF PORE PRESSURE GENERATION USED IN ANALYSIS

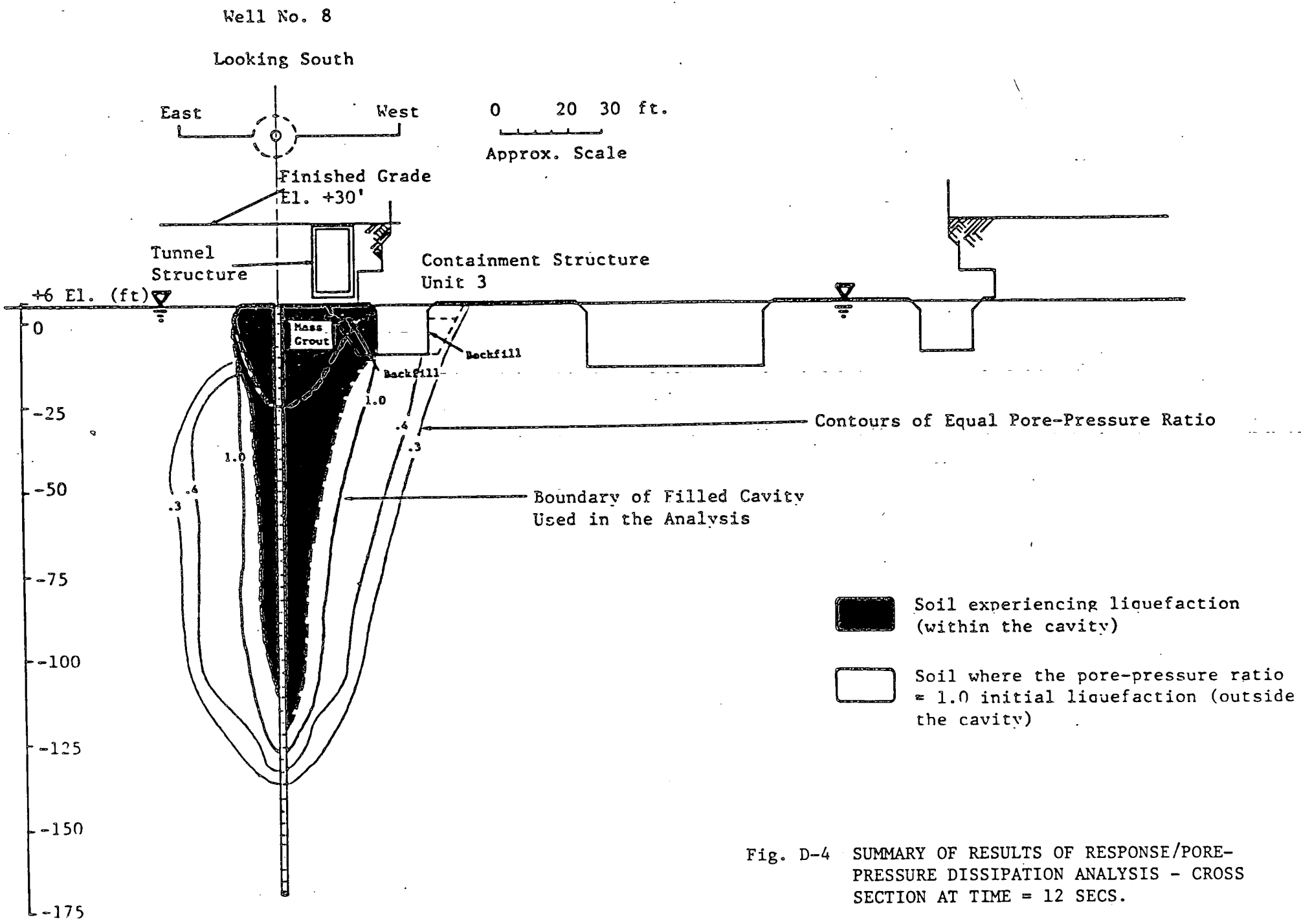

Fig. D-4 SUMMARY OF RESULTS OF RESPONSE/PORE-PRESSURE DISSIPATION ANALYSIS - CROSS SECTION AT TIME = 12 SECS.

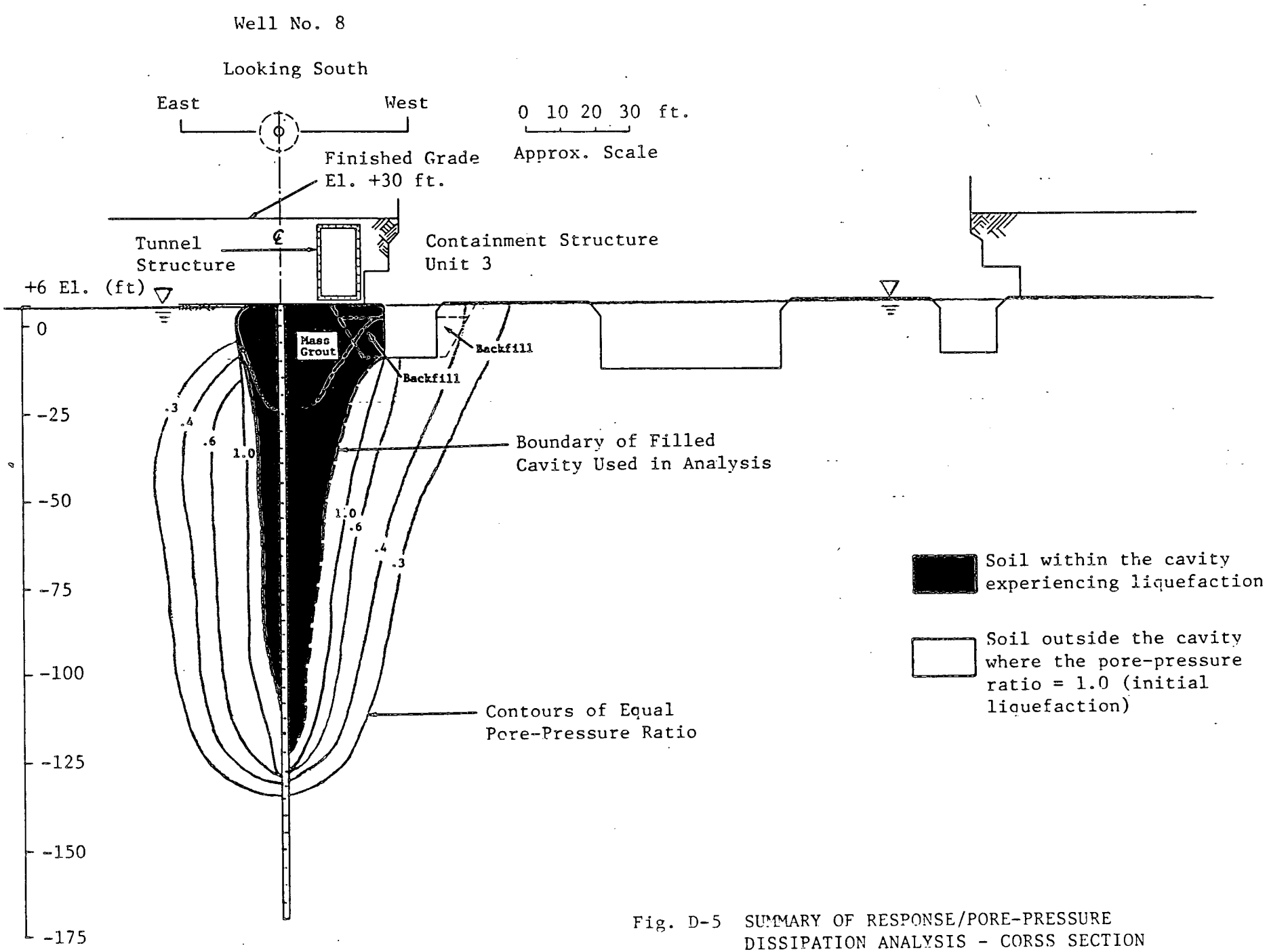

Fig. D-5 SUMMARY OF RESPONSE/PORE-PRESSURE DISSIPATION ANALYSIS - CORSS SECTION AT TIME = 30 SECS.

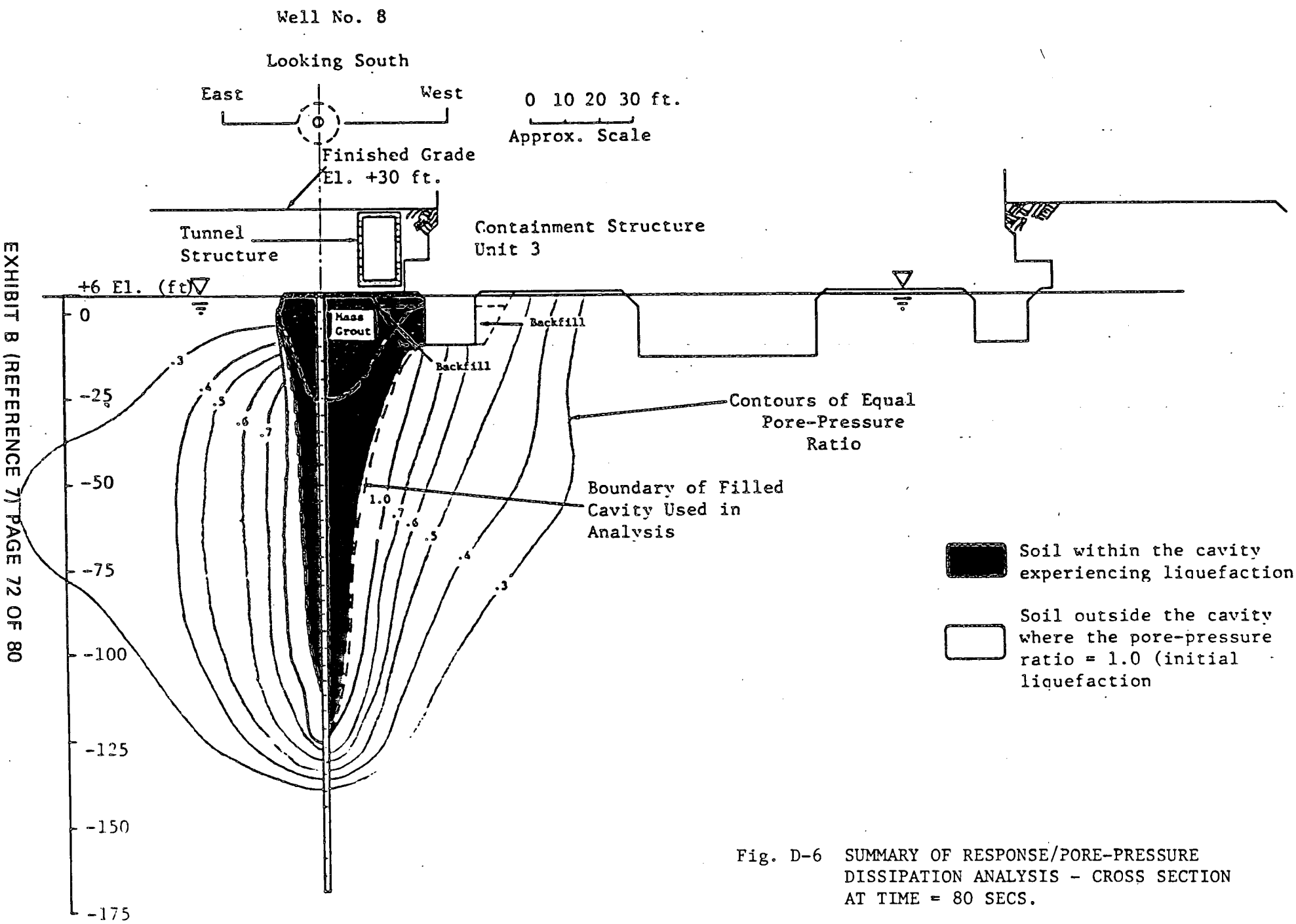

Fig. D-6 SUMMARY OF RESPONSE/PORE-PRESSURE DISSIPATION ANALYSIS - CROSS SECTION AT TIME = 80 SECS.

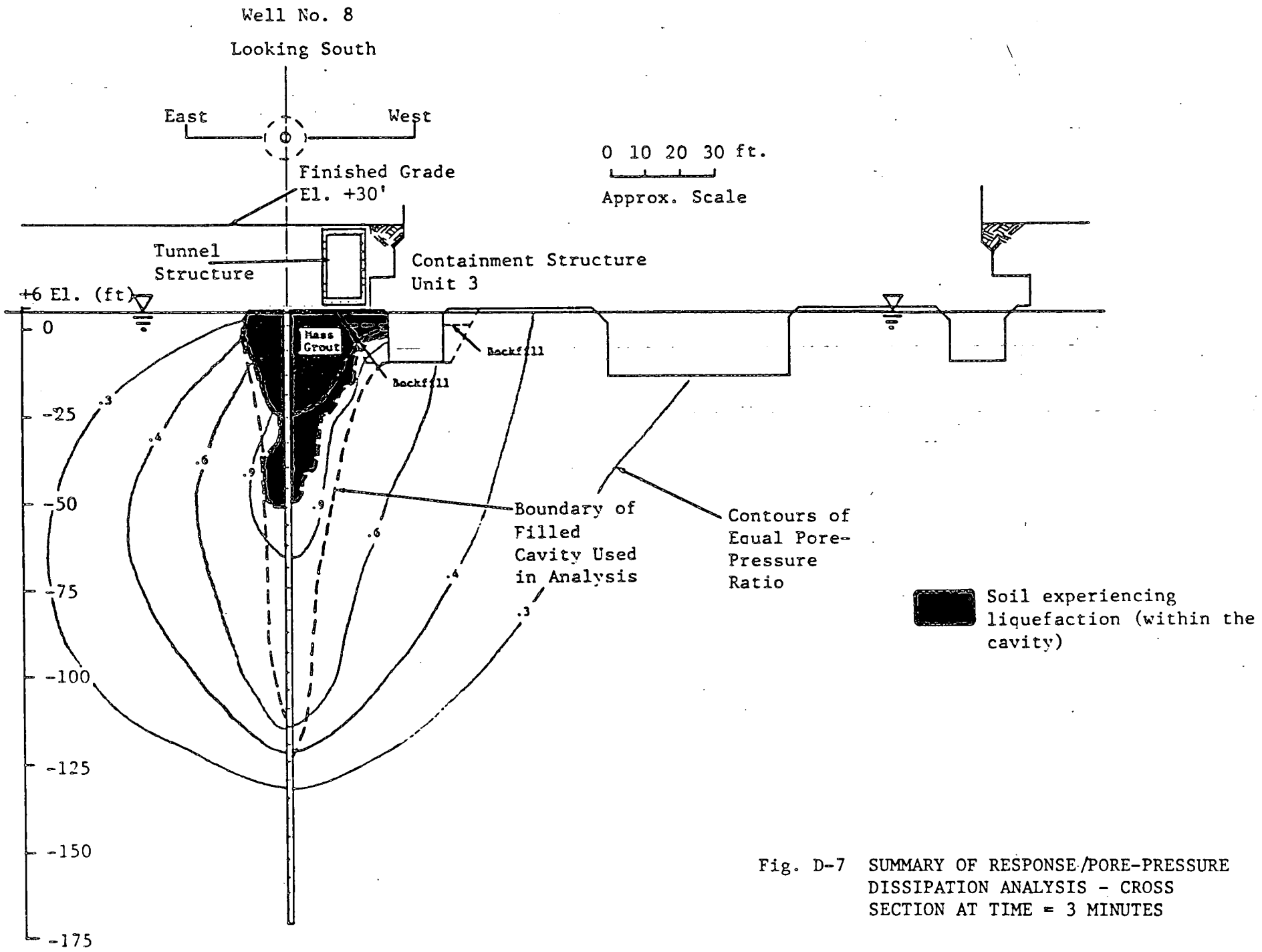

Fig. D-7 SUMMARY OF RESPONSE/PORE-PRESSURE DISSIPATION ANALYSIS - CROSS SECTION AT TIME = 3 MINUTES

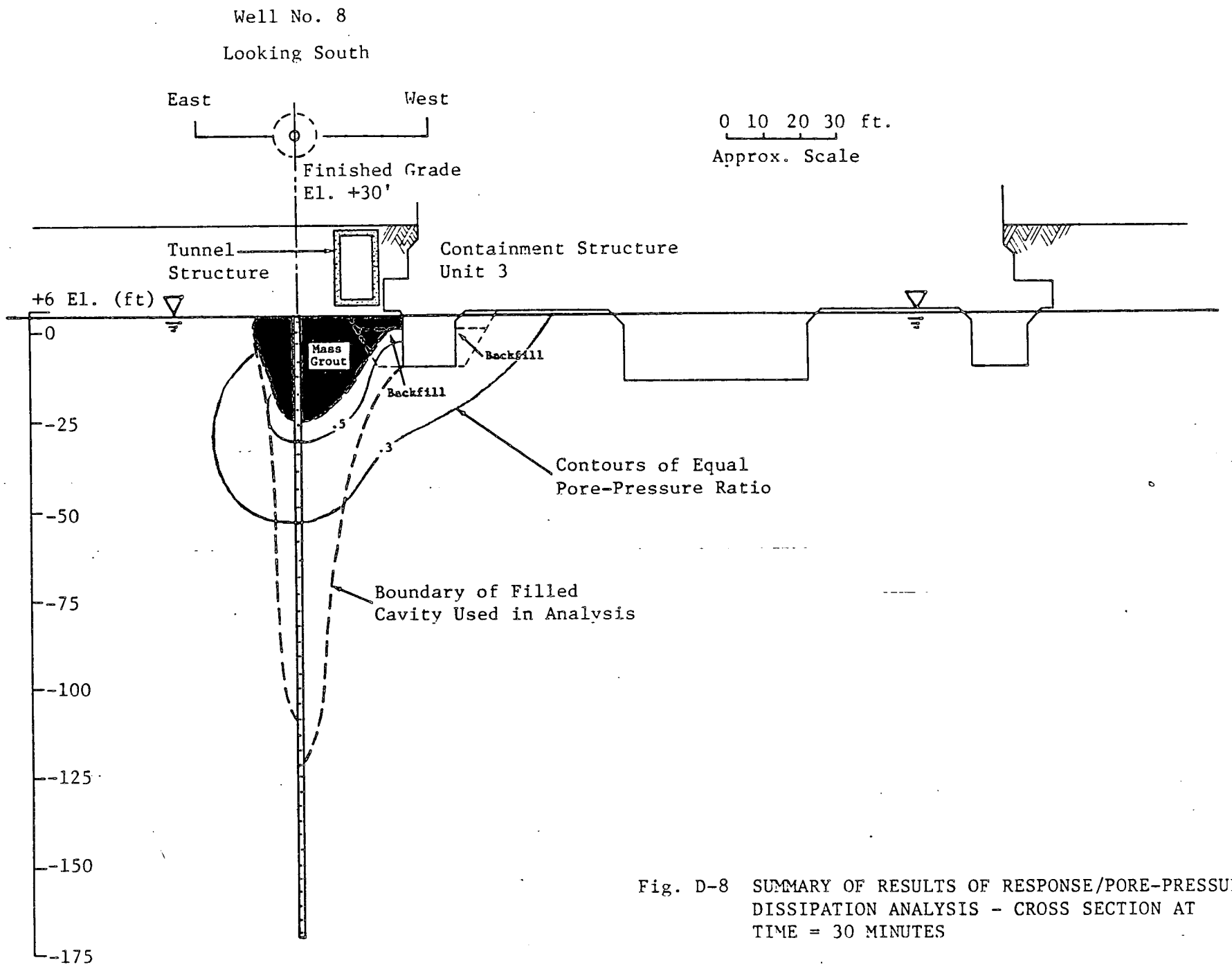

Fig. D-8 SUMMARY OF RESULTS OF RESPONSE/PORE-PRESSURE DISSIPATION ANALYSIS - CROSS SECTION AT TIME = 30 MINUTES

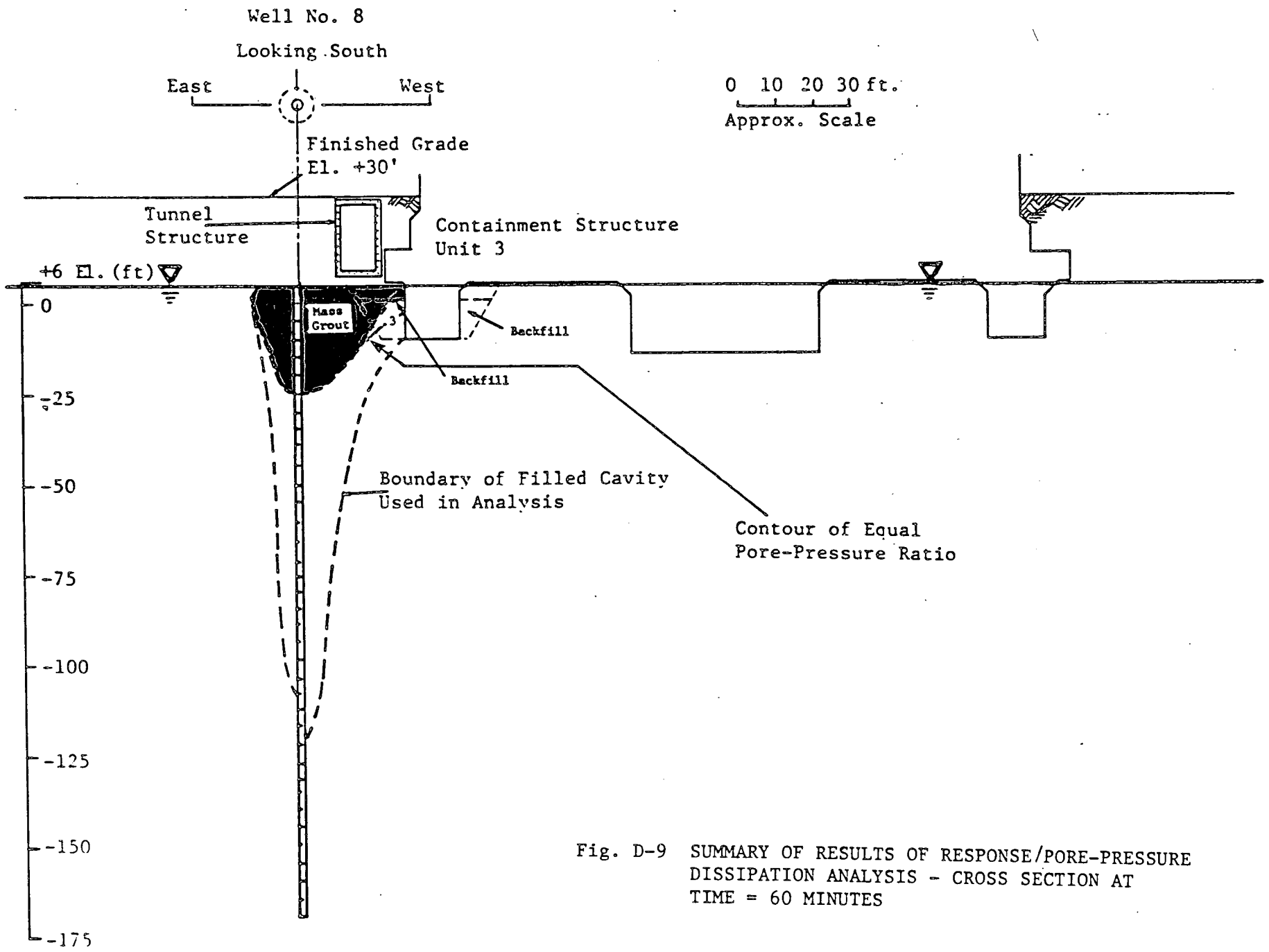

Fig. D-9 SUMMARY OF RESULTS OF RESPONSE/PORE-PRESSURE DISSIPATION ANALYSIS - CROSS SECTION AT TIME = 60 MINUTES

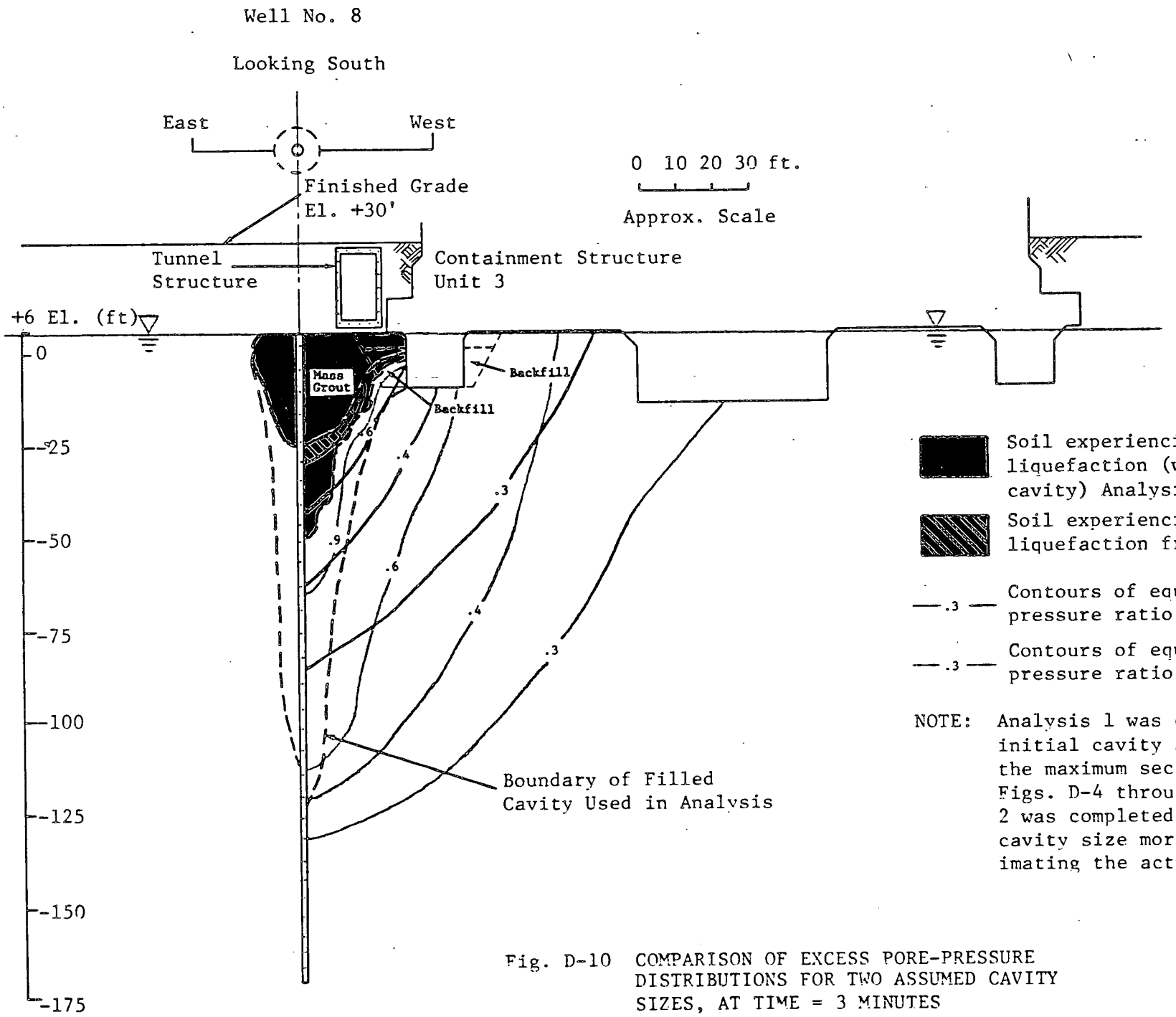

Fig. D-10 COMPARISON OF EXCESS PORE-PRESSURE DISTRIBUTIONS FOR TWO ASSUMED CAVITY SIZES, AT TIME = 3 MINUTES

APPENDIX E
ANALYSIS OF THE EFFECTS ON STRUCTURES

E.1 GENERAL APPROACH

The effects of the cavity at Well 8 on the static and seismic response of the Unit 3 Containment structure have been assessed. The assessment was made by comparing the size and proximity of the cavity to structures to that of the surrounding native San Mateo Sand that dominates in the static and seismic response of the structures.

The mass of native San Mateo Sand that dominates the seismic response of the structures has been demonstrated to be that soil within one radius of the structure as documented in Appendix 3.7C of the FSAR. A reasonable lateral boundary for this volume of soil was assumed to be that enclosed by a plane subtended from the edge of the structure at an angle of 45 degrees. Therefore, the mass of native soil that dominates the seismic response of the structure was assumed to be enclosed in a frustrum of a right circular cone centered on the structure with a top diameter equal to that of the base diameter of the structure, with a height equal to the radius of the structure, and with side surfaces inclined at 45 degrees as shown in Figure E-1. In considering the cavity at Well 8 and the Unit 3 Containment structure, the model shown on Figure E-1 contains better than 99% of the cavity and should therefore yield conservative results over those determined including the properties of soils below the one radius depth. Also because the soil near the base of the containment will experience higher stresses from the structure in comparison to its confining pressure than deeper portions of the soil mass, it will play a more important role in the support of the structure. Therefore, we have chosen to weight the importance of the soil with depth linearly from a factor of I = 1 at the surface to zero at a depth of one radius as shown on Figure E-1.

To evaluate the effects of a filled cavity on the overall stiffness of the supporting medium, the ratio of several geometric properties of the cavity to those of the dominant supporting soil as shown in Figure E-1 were studied. Specifically, four property ratios were considered as follows: (1) the ratio of the projected plan area of the cavity within a plane subtended at 45 degrees from the edge of the containment to that of the base area of the structure (a/A from Figure E-1); (2) the ratio of the volume of the cavity to that of the supporting soil extending to one radius below the structure within the 45 degree planar surface; (3) the ratio of the sum of area moments of inertia of the cavity from an axis of rotation through the center of the structure at 10 feet depth intervals to that of the supporting soil extending one radius below the structure; and (4) the ratio of mass moments of inertia of these same elements. The property ratios (1) and (2) described maximum effects of the cavity on the static and seismic vertical translation response of the structure relating to the compression and inertia of the soil masses, respectively. Properties (3) and (4) describe the maximum effects of the cavity on the static and seismic rotational response of the structure, relating to the bending resistance (rotational compression) and rotational inertia of the soil masses, respectively. By assuming zero stiffness of the soil within the cavity the property ratios equal directly the effective overall reduction in stiffness of the supporting soil mass.

E.2 EFFECT ON THE STRUCTURE USING THE RESPONSE AND PORE PRESSURE DISSIPATION ANALYSES

In the case of the response and pore pressure dissipation analyses the soil within the contour of pore pressure ratio equal to 1.0 (pore pressure = effective confining pressure, or initial liquefaction) the stiffness of the soil was assumed to reduce to zero. For the soil between the 0.3 to 1.0 contours of pore pressure ratio (Figures 8 through 11 for t = 80 seconds), the

stiffness of the soil was assumed to be reduced by the average reduction in effective confinement. Because shear modulus of the native soil is proportional to the confinement to the two-thirds power (Figure 3) the loss of stiffness was calculated by the expression:

$$\text{Stiffness Loss} = 1 - (1 - r_u)^{2/3}$$

where r_u = pore pressure ratio

The properties of the areas between the 0.3 and 1.0 contours of pore pressure ratio are therefore multiplied by the stiffness loss factor and added to the properties of the areas within 1.0 contour. To incorporate the effects of pore pressure ratio below 0.3 an additional reduction was included based on an inspection of average pore pressures of soil elements within the soil mass dominating in the support of the structure (Figure E-1). The resulting property value for the cavity and adjacent area softened by pore pressure is then divided by the total property for the mass of supporting soil to obtain the final property ratio. Property ratios calculated using the results summarized in Appendix C for the soil response and pore pressure dissipation parameters are summarized on Table 1.

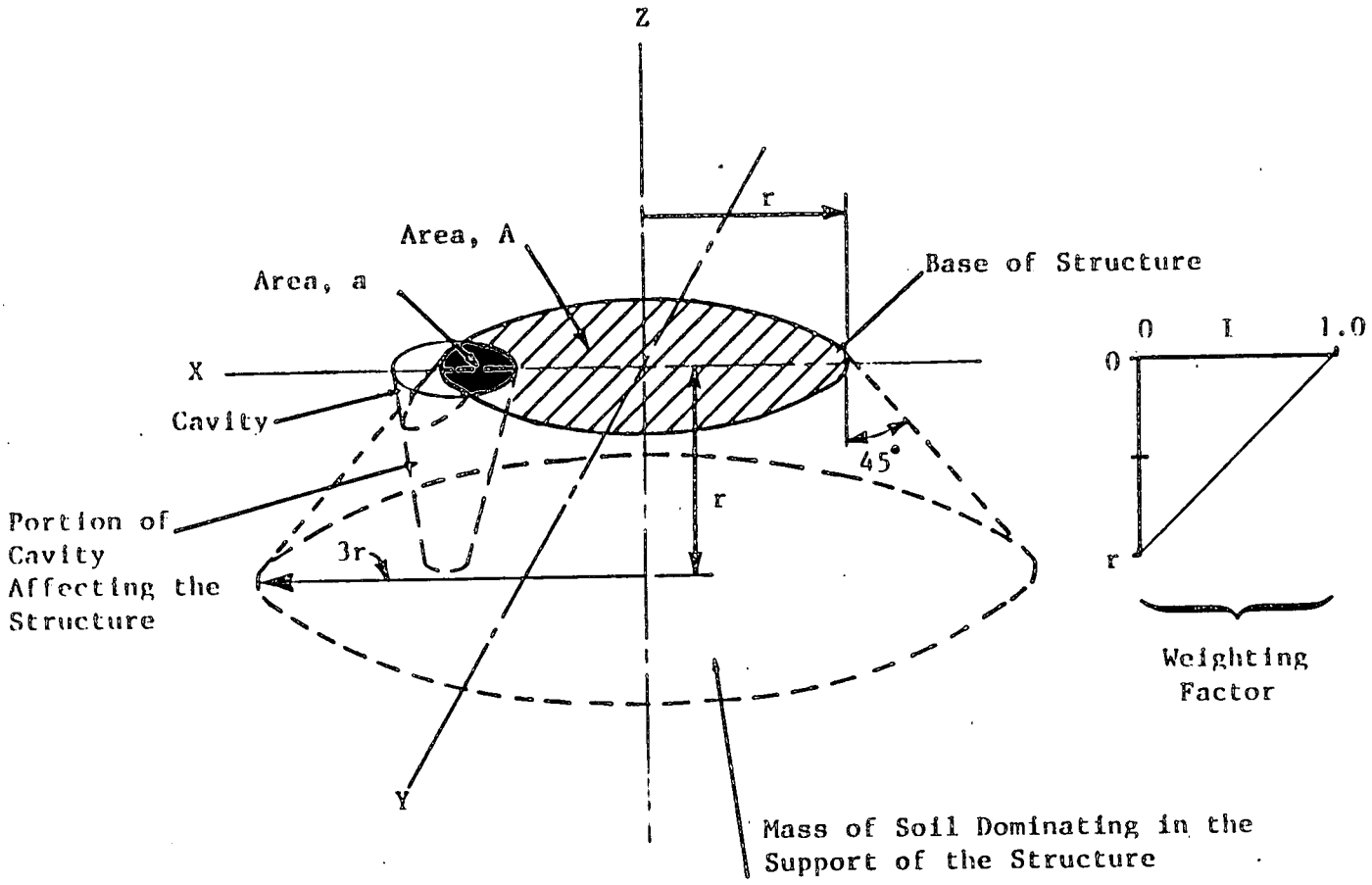

Fig. E-1 DIAGRAM DESCRIBING THE EFFECT OF THE CAVITY ON THE STRUCTURE

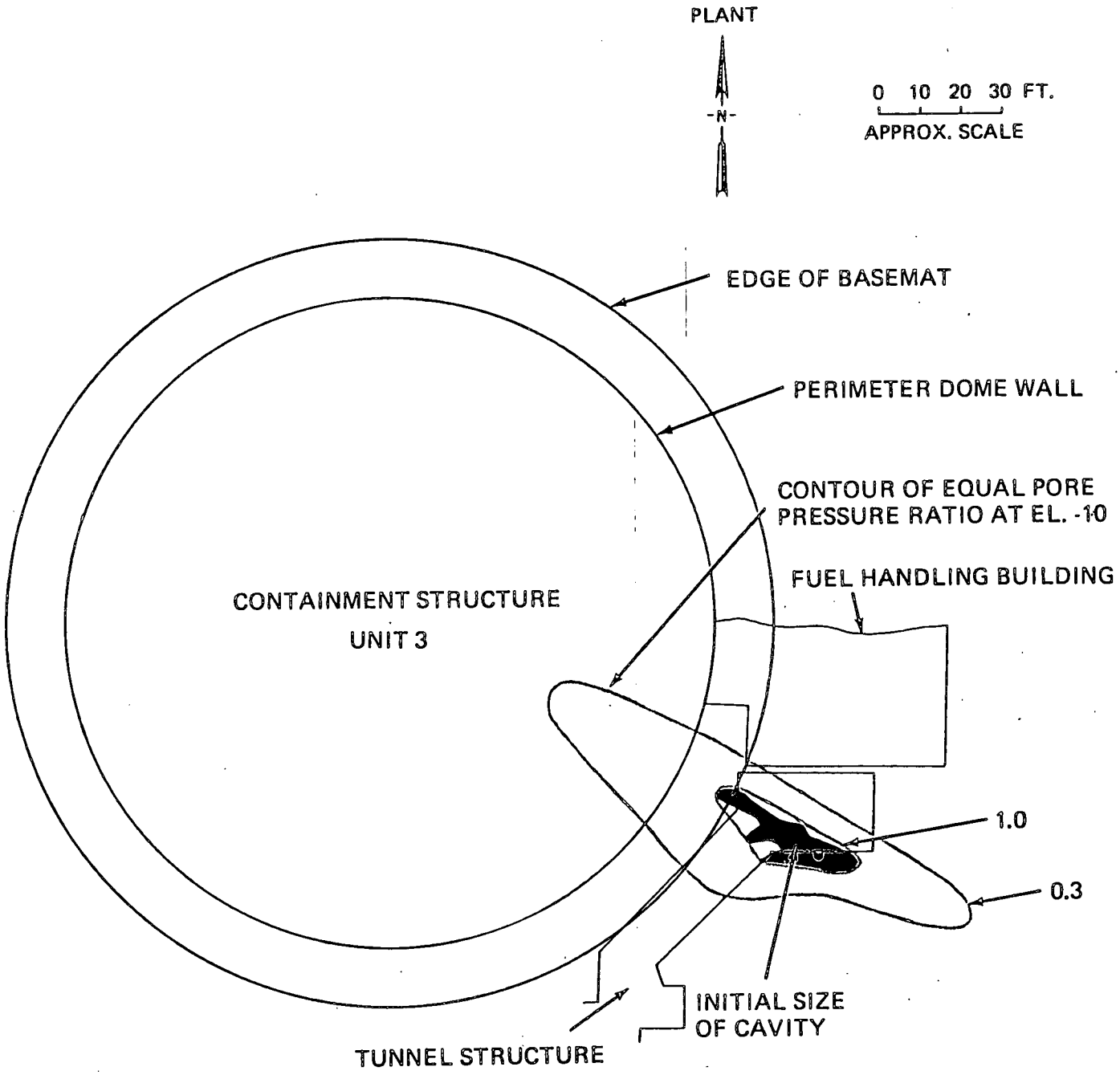

EXHIBIT C (REFERENCE 27)

Plan Section of Cavity and Pore Pressure Ratios = 0.3 and 1.0
at Elevation -10 Feet for Well 8,
San Onofre Nuclear Generating Station, Units 2 and 3

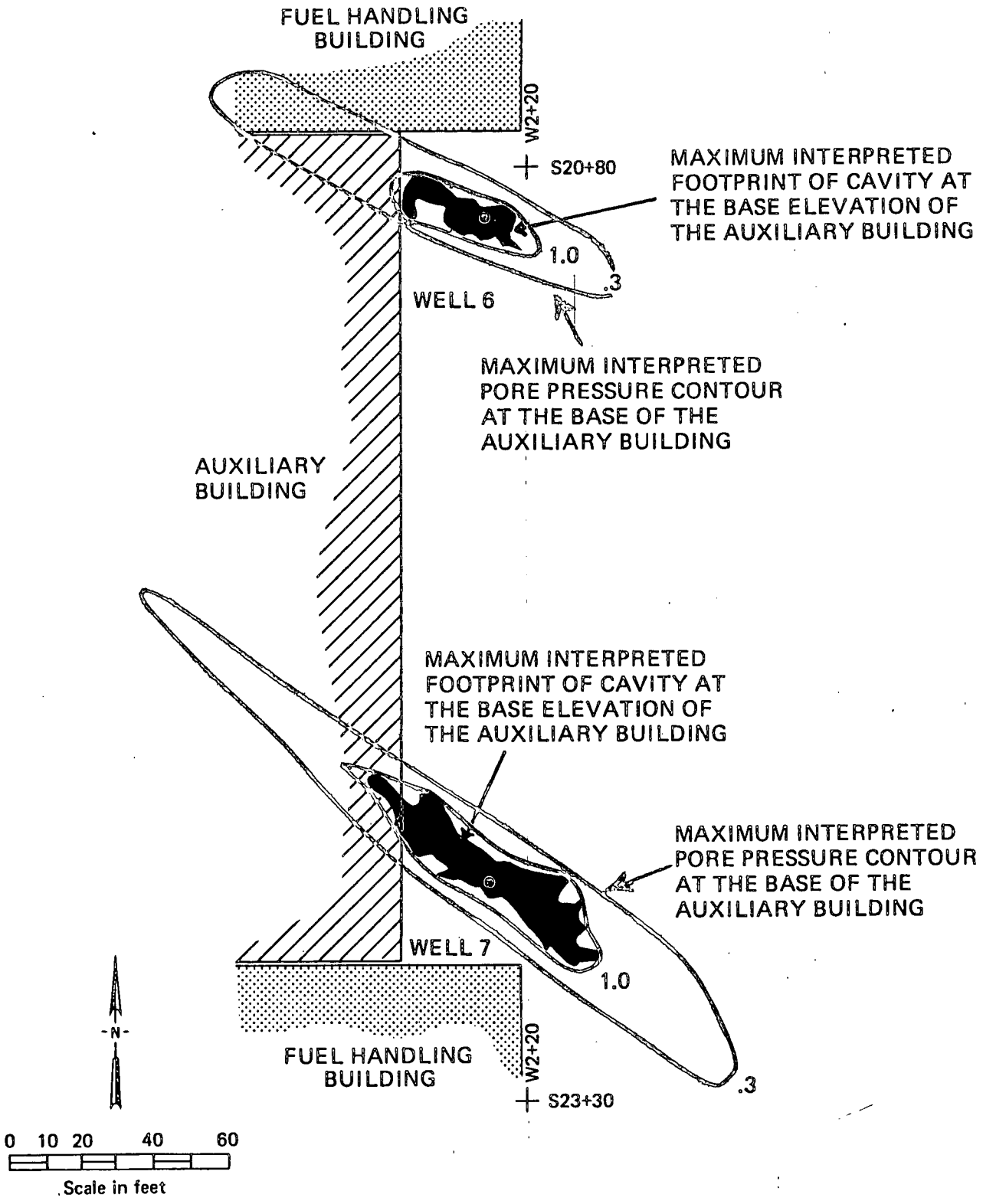

EXHIBIT D (REFERENCE 28)

Plan Section of Cavity and Pore Pressure Ratios = 0.3 and 1.0
at Elevation 0 Feet for Wells 6 and 7,
San Onofre Nuclear Generating Station, Units 2 and 3

SUMMARY OF MAXIMUM EFFECTS OF CAVITIES ON STRUCTURES

Structure	Well No.	Maximum Decrease of Dynamic Stiffness* (percent)		Maximum Increase in Settlement of Structure (percent)	
		Translation	Rocking	Total Vertical	Differential
Containment Unit 3	8	4	5	4	5
Auxiliary Units 2 and 3	6,7	2	2	2	2
Fuel Handling Unit 2	6	<1	3	<1	3
Fuel Handling Unit 3	7,8	<1	8	<1	8

* Affecting dynamic response of the structure during earthquake shaking.

EXHIBIT F (REFERENCE 29)

Maximum Interpreted Effect of the Cavity on the Tunnel Structure,
San Onofre Nuclear Generating Station, Units 2 and 3